AMERICAN UNIVERSITY OF BEIRUT

Model for Lattice Thermal Conductivity of Clamped and Free Surface Cylindrical Nanowires

by
LOUBNAN FOUAD ABOU HAMDAN

A thesis
submitted in partial fulfillment of the requirements
for the degree of Master of Science
to the Department of Physics
of the Faculty of Arts and Sciences
at the American University of Beirut

Beirut, Lebanon
July 2019

AMERICAN UNIVERSITY OF BEIRUT

Model for Lattice Thermal Conductivity of Clamped and Free Surface Cylindrical Nanowires

by

LOUBNAN FOUAD ABOU HAMDAN

Approved by:

Dr. Michel Kazan, Professor Physics	Advisor
Dr. Mounib El Eid, Professor Physics	Member of Committee
Dr. Malek Tabbal, Professor Physics	Member of Committee

Date of thesis defense: July 12, 2019

AMERICAN UNIVERSITY OF BEIRUT

THESIS, DISSERTATION, PROJECT RELEASE FORM

Student Name: ABOU HAMDAN LOUBNAN FOUAD
Last First Middle

⊗ Master's Thesis ○ Master's Project ○ Doctoral Dissertation

☒ I authorize the American University of Beirut to: (a) reproduce hard or electronic copies of my thesis, dissertation, or project; (b) include such copies in the archives and digital repositories of the University; and (c) make freely available such copies to third parties for research or educational purposes.

☐ I authorize the American University of Beirut, to: (a) reproduce hard or electronic copies of it; (b) include such copies in the archives and digital repositories of the University; and (c) make freely available such copies to third parties for research or educational purposes after: **One ___ year from the date of submission of my thesis, dissertation or project.**
Two ___ years from the date of submission of my thesis , dissertation or project.
Three ___ years from the date of submission of my thesis , dissertation or project.

L. ABOU HAMDAN 7/15/2019
Signature Date

This form is signed when submitting the thesis, dissertation, or project to the University Libraries

Acknowledgements

To Prof. Michel Kazan. An idol, mentor, and dear friend.

An Abstract of the Thesis of

Loubnan Fouad Abou Hamdan for Master of Science
Major: Physics

Title: Model for Lattice Thermal Conductivity of Clamped and Free Surface Cylindrical Nanowires

A model for the prediction of thermal conductivities of cylindrical nanowires (NWs) is presented. The model is based on the solution of the Boltzmann equation within the relaxation time approximation. Silicon (Si) NWs with clamped and free surface boundary conditions are considered, where the phonon group velocities were obtained from elasticity theory. Surface roughness is also modelled through the use of a specularity parameter. Calculations were carried out on NWs of diameter 10 and 22 nm for both clamped and free surface boundary conditions. The thermal conductivity of the NWs is found to be about two orders of magnitude lower than that of bulk Si. The significant drop in the thermal conductivity from its bulk value is ascribed to enhanced phonon boundary scattering and to phonon spectrum modification. The accuracy of the developed theory is demonstrated with reference to reported experimental measurements on individual Si NWs. It is found that the thermal conductivity of a free surface NW is larger than that of a clamped surface NW, and we predict an increase of $\sim$100% at 300 K for the 10 nm wire as the boundary conditions are changed from clamped to free. We suggest using the observed surface effect for thermal current modulation with piezoelectric cladding materials.

Contents

List of Figures

Chapter 1

Introduction

Device engineers have been remarkably successful at maintaining Moore's law, which states that the individual device components get smaller every year. The size of Metal-Oxide-Semiconductor Field-Effect Transistors (MOSFETs) for example, has been scaled down to a gate length of 20 nm, and an even smaller size is projected in the near future. The recent developments in synthesis and processing have allowed the routine production of such well-characterized materials with dimensions that vary on the length scale of a few nanometers. As the size of devices and structures shrinks down to the nanoscale, thermal management and manipulation become an increasingly pressing issue even though the primary goal of the device may not be thermal. For instance, in some devices, such as computer processors or semiconductor lasers, one wants to get the heat away as efficiently as possible, these systems require a high thermal conductivity. In others, such as thermal barriers or thermoelectric materials used for solid-state refrigeration, one wants the thermal conductivity to be as small as possible. Thus it is apparent that this perpetual size decrease in devices and the increase in their operating speeds and frequencies–which inevitably affect the thermal conditions imposed upon them, require a refined understanding of thermal transport at the nanoscale. This, in turn, warrants a deep investigation combining theoretical modeling, computational simulation, and experimental studies.

The understanding of heat conduction in low dimensional systems is not only significant for application and technological purposes, but it is also appealing from a scientific point of view, as heat conduction is one of the most important fundamental physical phenomena in nature. Traditionally, heat flux through a homogeneous material is believed to follow Fourier's law of heat conduction, which states that the heat flux is proportional to the temperature gradient along the path of heat flow, as $Q = -\kappa \nabla T$, where κ is the thermal conductivity which is a property of the material. The validity of Fourier's law has been well established for bulk materials, i.e three-dimensional macroscopic systems, however, it was found that heat conduction in nanostructures deviates from Fourier's law [5–7].

This is attributed to the fact that the length scales associated with the energy carriers (phonons, electrons, holes, etc.) become comparable to or larger than the characteristic length of the nanostructure [8].

The presence of boundaries and surfaces in nanostructures results in phenomena such as particle confinement, rarefaction, and surface reflection and transmission that alter the heat conduction. Thus, the thermal conductivity of low dimensional structures is no longer an intensive property of the material, which is the case for their bulk counterparts, but is dependent on the size and geometry of the structure and is usually diminished in comparison to the bulk thermal conductivity. This has lead to the development of various analytical models to describe heat transport in nanomatrials. In addition, approaches based on numerical solutions of the Boltzmann transport equation (BTE) and atomic-level simulations are used in the prediction of thermal conductivity. Various other simulation approaches, such as molecular dynamics (MD), Monte Carlo methods (MC), lattice dynamics (LD), and non-equilibrium Green's function methods (NEGF), have been implemented in investigating nanoscale thermal transport phenomena. Moreover, advances in micro- and nano-technology have enabled more and more experimental measurements of thermal properties of nanomaterials to be reported.

In this introductory chapter we attempt to provide a brief but concise review of the developments in the applied physics of nanoscale thermal transport that have resulted from advances in experiment, theory, and simulation over the past decade.

The current understanding of heat conduction in nanostructures is based on two different approaches. The first is based on the use of molecular dynamics (MD) simulations [9]. This method requires a model for the interatomic potential, which may be obtained from a fit based on phonon dispersion relations. To account for phonon-phonon interactions the interatomic potential is expanded up to at least third order. The most common way to employ MD simulations to calculate heat flow is to connect each end of the nanostructure to heat baths with different temperatures and then calculate the steady state flow of heat from one bath to the other. MD simulations have been particularly successful at modelling heat flow across interfaces and superlattices [10, 11]. In these cases molecular dynamics simulations are advantageous, as it is simple to model various aspects of the microscopic structure of an interface, such as the roughness and mixing [12, 13]. MD simulations thus present a powerful tool to model thermal transport in nanostructures. However, their atomistic approach– though being a fundamental one, poses simulation difficulties. In some nanostrutures the number of atoms that need to be included in the simulation may be rather large, and thus simulations of this kind may not be practical, at least with

the present computational power. Another limitation of MD simulations is that the calculations are purely classical. The average energy of each phonon mode is therefore taken to be $k_B T$, whereas the correct energy distribution should be given by the Planck distribution. This makes it difficult to model heat transport for frequencies where $\hbar\omega > k_B T$, and thus makes it almost impossible to appropriately account for quantum mechanical effects at low temperatures. This has prompted several attempts to correct molecular dynamics for quantum effects, most notably by applying quantum corrections to classical predictions of thermal conductivity [14]. However, these corrections were implemented at high temperatures where quantum effects are unimportant.

The second approach is based on the phonon Boltzmann equation which gives the total rate of change of the phonon distribution function $N_{\mathbf{k}s}$, where $\mathbf{k}$ is the wave vector, and s is an index labeling the phonon polarization. The total rate of change is split into two terms. The first term gives the rate at which the phonon distribution changes due to scattering $\partial N_{\mathbf{k}s}/\partial t|_{scatt}$, and the second provides the change due to diffusion. In the steady state regime the total rate of change of the phonon distribution function is set to zero and the Boltzmann equation is solved for $N_{\mathbf{k}s}$. The acquired distribution function may then be used to evaluate the phonon energy distribution and various thermal properties of the structure, particularly the lattice thermal conductivity. To solve the Boltzmann equation one needs to know the phonon dispersion relation, the group velocity, and the rate at which scattering occurs. The phonon dispersion relations can be obtained experimentally by neutron scattering, and inelastic X-ray scattering [15]. They may also be found analytically by making use of continuum approximations. Once the dispersion relations are attained, the group velocity is found by $\mathbf{v_{ks}} = \partial\omega(\mathbf{k}s)/\partial\mathbf{k}$. The scattering term on the other hand is much harder to evaluate and is usually approximated by a relaxation time $\tau(\mathbf{k}s)$ as $\partial N_{\mathbf{k}s}/\partial t|_{scatt} = (\overline{N}_{\mathbf{k}s} - N_{\mathbf{k}s})/\tau(\mathbf{k}s)$, where $\overline{N}_{\mathbf{k}s}$ is the Planck equilibrium distribution function.

In the relaxation time approximation various scattering mechanisms can be individually studied and their scattering rates are calculated by considering the anharmonic terms in the crystal Hamiltonian as perturbations and applying time dependent perturbation theory. It is found that first order perturbation theory performed on the third order terms in the crystal Hamiltonian results in three phonon interactions in which a phonon may decay into two phonons or two phonons may be annihilated and a third phonon is created. Likewise, second order perturbation on the third order terms and second order perturbation theory on the quartic terms in the Hamiltonian result in four phonon processes. However these are extremely rare except at very high temperatures and are estimated to be at least two or three orders of magnitude weaker than three phonon processes [2]. Three phonon processes are of two types: Normal three phonon processes (N-processes) and Umklapp three phonon processes (U-processes). N-

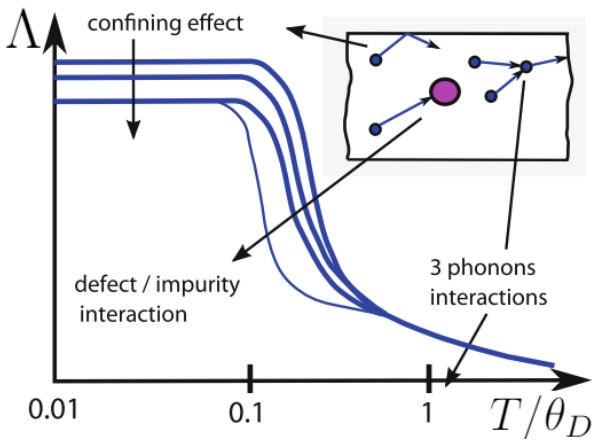

Figure 1.1: Temperature dependence of the mean free path $\Lambda = v_g\tau$ in a material, reproduced from [1].

processes conserve phonon momentum, while U-processes do not, thus the latter type of collisions directly reduces the heat flow, since they change the direction of the resulting phonon (or phonons) after collision, creating a thermal resistance. Other scattering mechanisms include point defect and isotope scattering, as well as phonon boundary scattering. The latter is especially prevalent in nanostructures due to the presence of borders and surfaces. Approximate expressions of the relaxation times for these scattering mechanisms in terms of phonon frequency were first given by Klemens *et al* [16–18] and are summarized in books by Ziman [19] and Srivastava [2].

The dependence of these scattering mechanisms with respect to temperature is as follows: at very low temperatures phonon boundary scattering dominates the phonon lifetime. At these temperatures the amplitude of atomic vibrations is minimal and thus phonons will travel in almost straight lines until they are scattered by the boundary. As temperature increases defect and impurity scattering become more efficient, which causes a decrease in the phonon mean free path (the average distance a phonon travels between two consecutive collisions). As temperatures increase further anharmonic phonon processes become predominant, and the mean free path decreases drastically as atomic vibrations become more and more rapid and the phonon suffers multiple internal collisions before it is even scattered by the boundary. The dependence of the phonon mean free path with respect to temperatures below and above the Debye temperature is illustrated in Figure 1.1.

The simplification of the Boltzmann equation by the relaxation time approximation allows the distribution function $N_{\mathbf{k}s}$ to be readily obtained, and thus the heat current is found from: $Q = \frac{1}{V}\sum_{\mathbf{k}s} N_{\mathbf{k}s}\mathbf{v}_{\mathbf{k}s}\hbar\omega(\mathbf{k}s)$, where V is the volume of

the solid. For cubic crystals the thermal conductivity is then given by the simple expression $\kappa = \sum_{\mathbf{k}s} C(\mathbf{k}s) v_{\mathbf{k}s}^2 \tau(\mathbf{k}s)$, where $C(\mathbf{k}s)$ is the contribution of the phonon $\mathbf{k}s$ to the specific heat. There are several well known difficulties with the use of this formula [19]. The major difficulty is that it is not clear whether every type of scattering process should be included in the calculation of $\tau(\mathbf{k}s)$. Anharmonic processes of the N-type do change the direction of the scattered phonon but leave the total flux of energy in a given direction essentially unchanged. Thus, one can argue that these processes do not contribute to the thermal resistance and so should be ignored and only U-processes considered. But if we suppose that there is a particular group of phonons which cannot be scattered in a U-process. Then, if N-processes are ignored, the thermal conductivity would be infinite, which is clearly impossible. To treat this situation correctly, it is necessary to go beyond the relaxation time approximation and include the effects of both N and U-processes in an appropriate way.

In order to account for the effect of N-processes, Callaway [20] proposed a model in which a modified relaxation time approach was employed. The collision term in the Boltzmann equation was split into two terms each having a different relaxation time. The first term includes the contribution due to the resistive processes that do not conserve momentum, such as U-processes. These tend to relax the phonon distribution to equilibrium so that they are included in the relaxation time approach as $(\overline{N} - N_{\mathbf{k}s})/\tau_U$, where $\overline{N}$ is the Planck equilibrium distribution, and τ_U is a relaxation time associated with the U-processes. On the other hand, since N-processes only cause the phonons to be displaced they were considered to relax the phonons to a displaced distribution function $N(\lambda)$, i.e their contribution to the rate of change of the distribution was written as $(N(\lambda) - N_{\mathbf{k}s})/\tau_N$, where λ is a constant vector in the direction of the temperature gradient, and τ_N is a relaxation time due to N-processes. Callaway assumed no distinction between longitudinal and transverse phonons and used a Debye approximation in which the phonon dispersion relation is linear. Through some assumptions, Callaway presented an integral expression of two terms κ_1 and κ_2 for the lattice thermal conductivity. The second term is considered an additional correction term to explain errors due to treating the normal processes as resistive ones and is usually neglected. The Callaway model is very successful at predicting the lattice thermal conductivity at low temperatures, and is widely used in various thermal conductivity calculations. Later, Holland [21] presented an analysis of thermal conductivity in which he considered the contribution of both longitudinal and transverse phonons to heat conduction under the assumption $\kappa_2 = 0$.

In the aforementioned models as well as in most calculations of thermal conductivity multiple scattering mechanisms are included in the relaxation time approximation by making use of the so-called Matthiessen rule, which states that the relaxation times for different scattering mechanisms are independent and thus

the contributions from each process are added inversely to the total relaxation time. The relaxation times used in [20, 21] are that of bulk materials, as the assumption used in solving the Boltzmann equation was that the phonon distribution function was spatially independent. For nanostructures the results of these models can be used provided some modifications are put into effect.

To calculate the heat flow in simple nanostructures, such as nanowires composed of a single material, it is sufficient to use the same phonon lifetimes as for a bulk material. This approach will break down only when the lateral dimensions of the structure become comparable to the phonon wavelength. However, the calculation of heat flow is much more difficult than for the bulk because now the phonon distribution function $N_{\mathbf{k}s}$ is spatially dependent. In a cylindrical nanowire, for example, the phonon distribution varies with distance r from the axis, and the solution for the phonon distribution function has to satisfy the Boltzmann equation at each value of r. Calculations for a diamond nanowire have recently been reported [22] by using an *ab initio* BTE calculation; it was necessary to make some approximations in order to reduce the simulation time that was needed. In a single-walled carbon nanotube (SWCNT), the situation is simpler, since the phonons only exist at one value of r. Calculations of the thermal conductivity in a SWCNT [23] and in graphene [24] have been performed by Lindsay *et al.*

As boundary scattering is predominant in nano-structures, special attention must be given to boundary scattering relaxation times. However, since three phonon processes and defect scattering all transpire in the volume of the crystal, while boundary scattering occurs at the surface, it remains unclear whether boundary scattering can be added in the Matthiessen rule. Nevertheless, boundary scattering is usually included in most calculations of lattice thermal conductivity by making use of the Casimir limit. Casimir [25] employed a radiation analogue and the Debye approximation to analyze phonon transport in a rod in the low temperature limit where internal scattering of phonons was negligible. The rod surface was treated as a blackbody that absorbed all the incident phonons and re-emitted phonons diffusely according to the local equilibrium distribution. Under these assumptions, the average phonon boundary scattering mean free path Λ_B is the diameter d for a circular rod, and $1.12w$ for a rod with a square cross section of width w. Thus in the Casimir limit the boundary relaxation time is always taken to be proportional to v/L, where v is the phonon group velocity and L is a characteristic length of the material.

Building upon Casimir's result and several others [26–28], Ziman [19] developed a solution of the phonon Boltzmann transport equation (BTE) in a rod under the relaxation time approximation. For diffuse boundary condition at the rod surface and absence of internal scattering, the boundary mean free path given

by the BTE solution [19] is the same as Casimir's result $\Lambda_{B,C}$, and is essentially an average over all orientations and positions of the distance traveled by phonon quasi-particles originated from the cross section and intercepted by the rod surface. For a partially specular and partially diffuse surface, a specular parameter p is used to describe the probability for specular scattering at the surface. Under the isotropic assumption, the phonon BTE can be solved to obtain the boundary scattering mean free path as $\Lambda_B = \Lambda_{B,C}(1+p)/(1-p)$ [19].

With internal scattering due to phonon-phonon processes or impurities accounted for, the BTE can be solved under the isotropic assumption to yield that the total mean free path Λ differs only slightly from that given by the Matthiessen rule, $1/\Lambda = 1/\Lambda_B + 1/\Lambda_i$ where Λ_i is the mean free path due to internal scattering processes [19]. Wang and Mingo [29] recently presented BTE solutions of Λ for nanowires of different cross sections and 2D nanoribbons with two diffuse edges, and verified the accuracy of the Matthiessen rule for the nanowire case.

These particle transport theories have been used to analyze the thermal conductivity data of nanostructures measured by a number of methods that have been established over the past decade [30, 31]. In addition to the axial thermal conductivity of different nanowire structures, the thermal conductivity of thin films [32] and periodic nanoporous membrane structures [33, 34] along the in-plane direction has been obtained with the use of suspended micro-devices with built in resistance thermometers [35]. The theoretical framework of Casimir and Ziman can explain quite well the suppressed thermal conductivity found in InAs nanowires [36, 37], Bi_2Te_3 nanowires [38], SnO_2 nanobelts [39], and Si nanowires [4] grown by a vapor liquid solid (VLS) method with a diameter larger than about 30 nm, as well as Bi nanowires [40], InSb nanowires [41], and SiGe nanowires [42] when additional impurity and defect scattering were considered. However, the boundary scattering is underestimated in these models, and the decrease in the calculated thermal conductivity can be attributed to the added defect and impurity scattering rather than the size effects, which are actually responsible for the decrease.

Using Callaway-type models, Mathiessen's rule, bulk phonon dispersion, and diffuse phonon-surface scattering, Wang and Mingo [43] and Shi [44], calculated the thermal conductivity for Si nanowires. Because the thermal conductivity of bulk Si is dominated by phonons with mean free paths longer than 100 nm, the size effect on the thermal conductivity can be readily observed in Si nanowires. As the relative thermal conductivity contribution of low-frequency phonons with long mean free paths is decreased by diffuse boundary scattering, the relative contribution from the high-frequency or short-wavelength zone boundary phonons increases in a nanowire. Consequently, the calculated thermal conductivity becomes more sensitive to the choice of the cutoff frequency in the Callaway-type

model for nanowires than for bulk crystals, and thus it is more sensitive to the dispersion relations used. The use of the same cutoff frequency as for bulk materials, combined with diffuse phonon-boundary scattering yields approximately the experimental thermal conductivity values reported by VLS Si nanowires with a diameter larger than 30 nm [4]. However the validity of this approximation becomes questionable when shorter nanowire diameters are considered. Moreover, these models do not seem to yield a sufficiently suppressed thermal conductivity for Silicon NWs of diameters less than or equal to 20 nm, such as the experimental measurements reported in [4].

Hence, in order to account for the measured reduction in the thermal conductivity of nanowires with diameters less than 30 nm in analytical calculations, it is critical to include surface roughness effects, various scattering mechanisms, spatial dependence of the phonon distribution, as well as accurate dispersion relations for the acoustic phonon modes in the nanostructure considered. We propose an analytical model based on the BTE and relaxation time approximation which includes all the aforementioned phenomena for the calculation of the thermal conductivity of cylindrical NWs. We use elasticity theory to obtain confined phonon group velocities in the cylindrical geometry. In addition, a summation over the modes along the lateral dimensions of the wire is effected. The model results are in excellent agreement with the experimental measurements and yield values for the thermal conductivity for Si NWs of 22 nm diameter that are extremely close to those presented in [4]. Further, the model results show that the thermal conductivity and thermal properties may be varied or tuned through the manipulation of the surface conditions of the NWs.

The outline of the thesis is as follows: In chapter 2 we touch on elements of phonon dispersion and present frequency spectra of confined phonons in clamped and free surface cylindrical nanowires. In chapter 3 we discuss the Boltzmann transport equation and give a solution to the equation in cylindrical coordinates within the relaxation time approximation. In chapter 4 we present the theory of lattice thermal conductivity based on the solutions to the Boltzmann equation, and we give an expression for the calculation of the thermal conductivity of cylindrical NWs. Our model results are then discussed in chapter 5 and compared with experimental data. Finally, we conclude in chapter 6 and discuss future work and investigation.

Chapter 2

Lattice dynamics and phonon dispersion

The conduction of heat in solids is mainly associated with elementary excitations called phonons. The relative motion of atoms in a solid generates these quasi-particles which carry thermal energy across it. Thus these phonons are directly related to the lattice dynamics of a crystal. By studying the deformation of a solid it is then possible to obtain a phonon spectrum or dispersion relation.

2.1 The harmonic approximation

The atoms in a solid may be visualized in terms of their ion cores and valence electrons. The ion cores vibrate about their equilibrium positions, and the valence electrons move about their ion cores. A first principles study of lattice dynamics is made possible by two approximations: an adiabatic approximation in which the ion cores are considered to be much heavier than the electrons so that their motion may be treated separately, and a harmonic approximation in which the crystal potential is only expanded up to harmonic terms.

Let us consider the total potential energy of a crystal in terms of interatomic potentials. The multi-body interactions in crystals are well approximated by pair or two-body interactions [2] represented by the potential $V(R)$, where R is the interatomic separation between a pair of atoms. We can expand $V(R)$ in a Taylor series in powers of small displacements $x = R - R_0$ around a minimum R_0

$$V(R) = V(R_0) + \frac{\partial V}{\partial R}\Big|_{R=R_0} x + \frac{1}{2}\frac{\partial^2 V}{\partial R^2}\Big|_{R=R_0} x^2 + ... \tag{2.1.1}$$

The first term is a constant, which is unimportant in dynamical problems. The second term vanishes in equilibrium, and thus we are left with the third term

which is quadratic in the displacement x. The consideration of only this term in the the potential is known as the harmonic approximation. In this approximation, an atom in a crystal can be described as a three dimensional simple harmonic oscillator, where the term $\frac{\partial^2 V}{\partial R^2}\Big|_{R=R_0}$ represents a force constant.

2.2 Phonons as crystal excitations

In the harmonic approximation the atoms of a crystal are visualized as joined by harmonic springs, so that the crystal dynamics are given by the linear combination of $3rN_0$ normal vibration modes (two transverse and one longitudinal mode), where N_0 is the number of unit cells and r is the number of atoms per unit cell of the crystal. A normal mode is expressed as a traveling wave of the form $Ae^{[i(\mathbf{k}.\mathbf{r}-\omega t)]}$, where $\mathbf{k}$ is the wave vector, ω is the frequency, and A is the amplitude of vibration. The energies of the normal modes in a crystal are given by that of a quantum harmonic oscillator i.e $\hbar\omega(\mathbf{k}s)\big(n+\frac{1}{2}\big)$, where s is an index labelling the polarization, and $n = 0, 1, 2....$

The quantum of energy $\hbar\omega(\mathbf{k}s)$ is associated with an elementary excitation called a phonon. Therefore, a phonon is a quantum of crystal vibrational energy. The phonon does not have a well defined momentum as it originates from the relative motion of atoms rather than the motion of their center of mass. However, for practical purposes we assign to each phonon a pseudo-momentum $\hbar\mathbf{k}$.

2.3 Phonon statistics

Phonons in crystals are considered as spin-less bosons in thermal equilibrium with each other. However, their number is not conserved since the number of phonon modes excited increases with temperature. Therefore the average number of phonons in the $\mathbf{k}th$ mode, in thermal equilibrium at temperature T is given by the Bose-Einstein distribution function with zero chemical potential

$$\overline{N}_{\mathbf{k}s} = \frac{1}{e^{\hbar\omega(\mathbf{k}s)/k_BT} - 1} \tag{2.3.1}$$

It is seen from (2.3.1) that at low temperatures the number of phonon modes tends to $e^{-\hbar\omega(\mathbf{k}s)/k_BT}$, and thus decreases exponentially with decreasing temperature until it reaches zero at absolute zero. At higher temperatures the number of phonons tends to $k_BT/\hbar\omega(\mathbf{k}s)$, and thus increases linearly with temperature.

In heat conduction problems a temperature gradient is applied along the crystal which causes phonons to be displaced from their equilibrium distribution function.

The phonon distribution function in this case will have the form

$$N_{ks} = \left[\exp(\hbar\omega(\mathbf{k}s)/k_B T - \psi_{\mathbf{k}s}) - 1\right]^{-1} \tag{2.3.2}$$

Where $\psi_{\mathbf{k}s}$ is a measure of the deviation from equilibrium distribution for phonons in the mode $\mathbf{k}s$. If heat conduction occurs slowly in the crystal i.e the rate of heat conduction is less than the period of atomic oscillations then the deviation from equilibrium represented by $\psi_{\mathbf{k}s}$ will be small.

In this case (2.3.2) can be expanded near $\psi_{\mathbf{k}s} = 0$, thus

$$\begin{aligned} N_{ks} &\approx \overline{N}_{\mathbf{k}s} + \psi_{\mathbf{k}s}\overline{N}_{\mathbf{k}s}(\overline{N}_{\mathbf{k}s} + 1) \\ &= \overline{N}_{\mathbf{k}s} + \widetilde{N}_{\mathbf{k}s} \end{aligned} \tag{2.3.3}$$

where $\widetilde{N}_{\mathbf{k}}$ is the deviated phonon distribution function. It is the phonons that are given by the deviated distribution function that actually contribute to the heat conduction across the material.

2.4 Phonon dispersion relations in a linear chain

In order to find the normal modes of a crystal the calculation of the phonon dispersion relations is required. The dispersion relations express the relationship between the frequency ω and the wave vector $\mathbf{k}$ of a wave, or alternatively, between the energy $\hbar\omega$ and the momentum $\hbar\mathbf{k}$ of a particle. They thus characterize the vibrational properties of a medium.

In the field of heat transfer, and more particularly, heat transport by conduction, i.e., through vibrations in crystal structures, the dispersion relations of a material are used to define the velocity of the heat carriers or phonons. Three velocities are defined as a function of the frequency and polarization of the wave: the group velocity v_g, the phase speed v_p, and the speed of sound v_s. The speed of sound can also be defined as the low frequency speed of acoustic modes, and the phase speed and group velocity tend to this quantity when ω is small

$$\mathbf{v}_g = \frac{d\omega}{d\mathbf{k}}, \quad v_p = \frac{\omega}{k}, \quad v_s = \lim_{\omega \longrightarrow 0} \frac{d\omega}{dk} \tag{2.4.1}$$

To illustrate the fundamental features of phonon dispersion we will first consider the simple case of a one dimensional lattice chain.

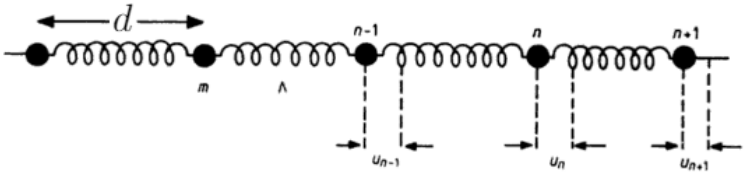

Figure 2.1: Monatomic linear chain showing displacements of the $(n-1)th$, nth, and $(n+1)th$ atoms from equilibrium [2]

Consider a monatomic linear chain of an infinitely large number of atoms N separated by a distance d. We will assume periodic boundary conditions in which the $(N+1)th$ atom is the first, and we consider that only nearest neighbor forces are significant.

The displacement of the nth atom is given by Newton's second law and Hooke's law

$$m\frac{d^2u_n}{dt^2} = \Lambda[(u_{n+1} - u_n) + (u_{n-1} - u_n)] \tag{2.4.2}$$

where m is the mass of an atom and Λ is the force constant.

We consider a solution of the form

$$u_n = Ae^{[i(knd-\omega t)]} \tag{2.4.3}$$

Inserting this in (2.4.2) we find

$$\omega = 2\sqrt{\frac{\Lambda}{m}}\left|\sin kd/2\right| \tag{2.4.4}$$

Equation (2.4.4) gives the dispersion relation of a monatomic linear chain and is shown in Figure 2.2.

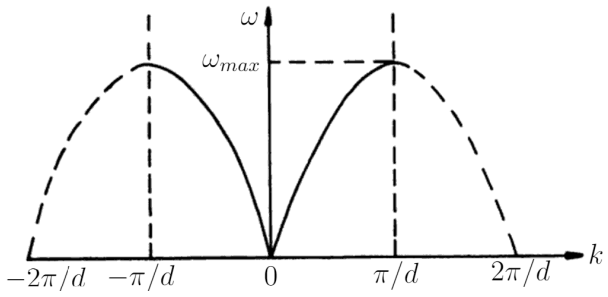

Figure 2.2: Phonon dispersion curve for the monatomic linear chain. The Brillouin zone is the region that extends from $-\pi/d$ to π/d

From the periodic boundary condition the allowable wave vectors are given by

$$k = \frac{2\pi n}{Nd}, \quad n = 0, \pm 1, \pm 2, ... \tag{2.4.5}$$

Since $k = 2\pi/\lambda$ it is seen that if $n > N/2$ then the wavelength λ will be less than twice the interatomic spacing, i.e there are no atoms between one period. However, atomic displacements in empty space, where there are no atoms, do not exist. Thus the allowable values of n for lattice vibrations lie between $-N/2$ and $N/2$. Therefore, the allowable wavevectors are confined to the Brillouin zone.

The phonon group velocity is also seen to vary from its maximum value $v_g = d\sqrt{\frac{\Lambda}{m}}$ at the zone center, which is the speed of sound in this case, to zero at the zone boundary so that the vibrational modes form standing waves at the edge of the Brillouin zone.

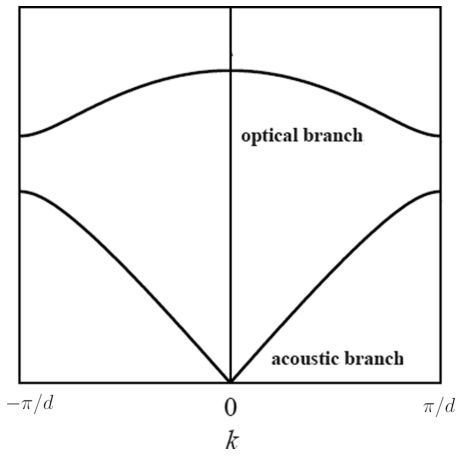

Figure 2.3: Phonon dispersion curve for the diatomic linear chain

In the case of a diatomic linear chain the dispersion curve becomes more complicated and the vibrational modes are split into two branches. As shown in Figure 2.3 these branches correspond to the acoustic and the optical phonon modes.

Lattice vibrations in the upper branch result from the two atoms in a unit cell vibrating opposite to each other. If two atoms had opposite charges on them they would result in the formation of a dipole, such a mode of vibration could thus be excited by an electric field of the appropriate frequency. For this reason the upper branch is called the optical branch. On the other hand, vibrations in the lower branch are due to the two atoms vibrating in phase, this is a characteristic of a sound wave, whence the lower branch is called the acoustic branch. It is easily seen that the optical phonons have very low group velocity which tends to

zero at both the zone center and boundary, as a result they do not conduct heat and are usually neglected when dealing with heat transport problems. Acoustic phonons on the other hand have large group velocity which only tends to zero near the zone boundary which makes them the main heat carriers in solids. Thus when finding dispersion relations of a real three dimensional medium it suffices to consider the dispersion of the acoustic phonons only.

2.5 Elastic waves in crystals

If we consider that there is a vibrational excitation in a solid with which we can associate an effective dimension λ and angular frequency ω, where λ may be a wavelength or some other characteristic length of the material, then if $\lambda \gg d$, where d is a mean interatomic spacing, the response of the medium to the excitation is essentially that of a continuum since, within the length λ there exists a large number of atoms. Thus in deriving the dispersion relations of acoustic phonons in a solid medium, the body may be considered as an elastic continuum in the long wavlength limit.

If the heat conduction in the solid occurs slowly, i.e the heat exchange during times in the order of the period of oscillatory motions in the body is negligible, then the deformations of the medium will be small and thus result in the formation of elastic waves. In order to obtain the equations of motion of an elastic medium we must equate the internal stress force $\partial\sigma_{ik}/\partial x_k$ to the product of the acceleration $\ddot{u}_i$ and the mass per unit volume of the body i.e it density ρ, where σ_{ik} is the stress tensor and u_i gives the displacement of any point in the solid:

$$\rho\ddot{u}_i = \frac{\partial\sigma_{ik}}{\partial x_k} \tag{2.5.1}$$

In general the stress tensor can be related to the strain tensor by a rank four tensor λ_{iklm} called the elastic modulus tensor, as

$$\sigma_{ik} = \lambda_{iklm}u_{lm} \tag{2.5.2}$$

where repeated indices are summed over, and u_{ik} is the symmetric rank two strain tensor:

$$u_{ik} = \frac{1}{2}\left(\frac{\partial u_i}{\partial x_k} + \frac{\partial u_i}{\partial x_k}\right) \tag{2.5.3}$$

Substituting this in (2.5.1) we find

$$\begin{aligned}\rho\ddot{u}_i &= \lambda_{iklm}\frac{\partial u_{lm}}{\partial x_k} \\ &= \frac{1}{2}\lambda_{iklm}\frac{\partial^2 u_l}{\partial x_k \partial x_m} + \frac{1}{2}\lambda_{iklm}\frac{\partial^2 u_m}{\partial x_k \partial x_l} \end{aligned} \tag{2.5.4}$$

Rearranging some dummy indices in (2.5.4) we obtain the general equations of motion of a crystal:

$$\rho\ddot{u}_i = \lambda_{iklm}\frac{\partial^2 u_m}{\partial x_k \partial x_l} \tag{2.5.5}$$

We consider monochromatic elastic waves in the crystal of the form

$$u_i = u_{i0}e^{i[\mathbf{k}.\mathbf{r}-i\omega t]} \tag{2.5.6}$$

where u_{i0} are constants defining the amplitude of vibration.

Substituting this solution into the general equation of motion gives

$$(\rho\omega^2\delta_{im} - \lambda_{iklm}k_k k_l)u_m = 0 \tag{2.5.7}$$

Here δ_{im} is the Kronecker delta. In order to obtain non-trivial solutions the determinant of the coefficients must vanish, i.e

$$|\rho\omega^2\delta_{im} - \lambda_{iklm}k_k k_l| = 0 \tag{2.5.8}$$

This is a cubic equation in ω^2 that gives the dispersion relations of a bulk crystal. It has three solutions that are in general different. Obtaining the dispersion relations from this equation is generally difficult since for different directions we obtain different solutions depending on the values of the components of the tensor λ_{iklm} which in turn depend on the symmetry of the crystal.

2.6 Elastic waves in an isotropic medium

If we consider an isotropic medium the equations of motion (2.5.1) are greatly simplified, since the components of the elastic modulus tensor are the same in all directions and the relation between the stress and strain tensor becomes

$$\sigma_{ik} = Ku_{ll}\delta_{ik} + 2\mu\left(u_{ik} - \frac{1}{3}\delta_{ik}u_{ll}\right) \tag{2.6.1}$$

Here, $K = \lambda + \frac{2}{3}\mu$ is the modulus of compression and λ and μ are Lame's constants [45].

Using this in (2.5.1) we obtain the general equation of motion for an isotropic elastic medium [45]:

$$\rho\ddot{\mathbf{u}} = \mu\nabla^2\mathbf{u} + (\lambda+\mu)\nabla(\nabla.\mathbf{u}) \tag{2.6.2}$$

We can rewrite this equation in the form

$$\ddot{\mathbf{u}} = c_t^2\nabla^2\mathbf{u} + (c_l^2 - c_t^2)\nabla(\nabla.\mathbf{u}) \tag{2.6.3}$$

where

$$c_t = \sqrt{\frac{\mu}{\rho}}, \quad \text{and} \quad c_l = \sqrt{\frac{\lambda+2\mu}{\rho}} \tag{2.6.4}$$

are the bulk transverse and longitudinal speeds respectively.

We consider a solution in the form

$$\mathbf{u} = \mathbf{u}_l + \mathbf{u}_t \tag{2.6.5}$$

with

$$\nabla \times \mathbf{u}_l = 0 \tag{2.6.6}$$
$$\nabla.\mathbf{u}_t = 0 \tag{2.6.7}$$

Thus we find

$$\ddot{\mathbf{u}}_l + \ddot{\mathbf{u}}_t = c_t^2\nabla^2(\mathbf{u}_l + \mathbf{u}_t) + (c_l^2 - c_t^2)\nabla(\nabla.\mathbf{u}_l) \tag{2.6.8}$$

If we take the divergence of the above equation, since $\nabla.\mathbf{u}_t = 0$, we get

$$\nabla.(\ddot{\mathbf{u}}_l - c_l^2\nabla^2\mathbf{u}_l) = 0 \tag{2.6.9}$$

And by (2.6.6) the curl of this expression vanishes as well, thus since the divergence and curl of this vector vanish, then the vector must vanish identically i.e

$$\ddot{\mathbf{u}}_l - c_l^2\nabla^2\mathbf{u}_l = 0 \tag{2.6.10}$$

Similarly, taking the curl of (2.6.8) and using (2.6.6) and (2.6.7), we find

$$\ddot{\mathbf{u}}_t - c_t^2\nabla^2\mathbf{u}_t = 0 \tag{2.6.11}$$

If we consider monochromatic elastic waves with frequency ω we obtain wave equations in $\mathbf{u}_l$ and $\mathbf{u}_t$:

$$\nabla^2 \mathbf{u}_l + \frac{\omega^2}{c_l^2}\mathbf{u}_l = 0, \quad \text{and} \quad \nabla^2 \mathbf{u}_t + \frac{\omega^2}{c_t^2}\mathbf{u}_t = 0 \tag{2.6.12}$$

For solutions of the form (2.5.6) we obtain the linear dispersion relations of a bulk isotropic medium:

$$\omega = c_l k, \quad \text{and} \quad \omega = c_t k \tag{2.6.13}$$

The first is the dispersion relation of the longitudinal phonon modes, while the second is the doubly degenerate dispersion relation for the two transverse modes.

2.7 Displacement vector of an isotropic solid cylinder

In order to describe the thermal conductivity $\kappa(T)$ of Si nanowires (NWs) we should take into account the modification of the acoustic phonon dispersion due to confinement induced by the boundary.

For small cross section NWs, typically below $\sim$ 8 nm, calculation of the size dependent phonon spectrum can be carried out by using MD simulations. For larger NW cross sections MD simulations become computationally prohibitive and the only way for calculating the size dependent phonon dispersion spectrum is the use of the elastic continuum approximation. Although the elastic continuum approximation is valid only for phonons of wavelengths much larger than the interatomic spacing, a number of experiments confirm its usefulness in describing qualitatively the effect of size on the Debye temperatures and phonon velocities [46–48].

Thus in order to obtain the phonon dispersion spectrum for NWs of cross-section ranging from 10 to 22nm in diameter we must solve the general equation of motion (2.6.3) in the cylindrical geometry.

We consider an isotropic elastic cylinder of radius a whose axis is directed along the z-axis and is assumed to be infinite in that direction. Let $\mathbf{u} = (u_r, u_\phi, u_z)$ be the components of the displacement of a point in the solid.

If we consider monochromatic waves with frequency ω, i.e a time dependence given by $e^{-i\omega t}$ then the equations of motion assume the form

$$-\omega^2 \mathbf{u} = c_t^2 \nabla^2 \mathbf{u} + (c_l^2 - c_t^2)\nabla(\nabla.\mathbf{u}) \tag{2.7.1}$$

In order to simplify the equations we look for solutions of the form

$$\mathbf{u} = \nabla\psi + \nabla \times \mathbf{H} \tag{2.7.2}$$

where ψ is some scalar and $\mathbf{H}$ is a vector potential defined up to a gauge transformation, $\mathbf{H} \longrightarrow \mathbf{H} + \nabla\varphi$, where φ is an arbitrary scalar field.

Inserting this in (2.7.1) and using the identity $\nabla(\nabla.\mathbf{H}) = \nabla^2\mathbf{H} + \nabla \times \nabla \times \mathbf{H}$ along with the fact that the divergence of the curl and the curl of a gradient both vanish, we obtain wave equations for both ψ and $\mathbf{H}$ i.e

$$\nabla^2\psi + k_l^2\psi = 0, \quad \nabla^2\mathbf{H} + k_t^2\mathbf{H} = 0 \tag{2.7.3}$$

where

$$k_l^2 = \frac{\omega^2}{c_l^2}, \quad \text{and} \quad k_t^2 = \frac{\omega^2}{c_t^2} \tag{2.7.4}$$

We assume the following solutions [49]

$$\psi = f(r)\cos(n\phi)e^{ikz} \tag{2.7.5}$$
$$H_r = h_r(r)\sin(n\phi)e^{ikz} \tag{2.7.6}$$
$$H_\phi = h_\phi(r)\cos(n\phi)e^{ikz} \tag{2.7.7}$$
$$H_z = h_r(r)\sin(n\phi)e^{ikz} \tag{2.7.8}$$

Inserting these solutions in (2.7.3) we find

$$\frac{d^2f}{dr^2} + \frac{1}{r}\frac{df}{dr} - \frac{n^2}{r^2}f - k^2f + k_l^2f = 0 \tag{2.7.9}$$

We define

$$\alpha^2 = k_l^2 - k^2 \tag{2.7.10}$$

thus the equation for $f(r)$ can be rewritten as

$$\frac{d^2f}{dr^2} + \frac{1}{r}\frac{df}{dr} + \left(\alpha^2 - \frac{n^2}{r^2}\right)f = 0 \tag{2.7.11}$$

This is Bessel's equation whose solution can be written as follows

$$f(r) = AJ_n(\alpha r) \tag{2.7.12}$$

where $J_n(\alpha r)$ are the ordinary Bessel functions of the first kind. Bessel functions of the second kind are precluded from the solution since they become infinite at $r = 0$.

For $h_z(r)$ we obtain a similar equation

$$\frac{d^2h_z}{dr^2} + \frac{1}{r}\frac{dh_z}{dr} + \left(\beta^2 - \frac{n^2}{r^2}\right)h_z = 0 \tag{2.7.13}$$

where,

$$\beta^2 = k_t^2 - k^2 \tag{2.7.14}$$

thus

$$h_z(r) = B_3 J_n(\beta r) \tag{2.7.15}$$

For h_r and h_ϕ we find two coupled equations

$$\frac{d^2h_r}{dr^2} + \frac{1}{r}\frac{dh_r}{dr} + \frac{1}{r^2}(-n^2h_r + 2nh_\phi - h_r) - k^2h_r + k_l^2h_r = 0 \tag{2.7.16}$$

$$\frac{d^2h_\phi}{dr^2} + \frac{1}{r}\frac{dh_\phi}{dr} + \frac{1}{r^2}(-n^2h_\phi + 2nh_r - h_\phi) - k^2h_\phi + k_l^2h_\phi = 0 \tag{2.7.17}$$

Subtracting (2.7.17) from (2.7.16) we find

$$\left[\frac{d^2}{dr^2} + \frac{1}{r}\frac{d}{dr} + \beta^2 - \frac{(n+1)^2}{r^2}\right](h_r - h_\phi) = 0 \tag{2.7.18}$$

The solution to this equation is

$$h_r - h_\phi = 2B_2 J_{n+1}(\beta r) \tag{2.7.19}$$

Adding (2.7.16) and (2.7.17) we obtain

$$\left[\frac{d^2}{dr^2} + \frac{1}{r}\frac{d}{dr} + \beta^2 - \frac{(n-1)^2}{r^2}\right](h_r + h_\phi) = 0 \tag{2.7.20}$$

the solution to this can be written as

$$h_r + h_\phi = 2B_1 J_{n-1}(\beta r) \tag{2.7.21}$$

Therefore,

$$h_r = B_1 J_{n-1}(\beta r) + B_2 J_{n+1}(\beta r) \tag{2.7.22}$$

$$h_\phi = B_1 J_{n-1}(\beta r) - B_2 J_{n+1}(\beta r) \tag{2.7.23}$$

In order to find the displacement vector $\mathbf{u}$ we only require three constants. However, our formulation has yielded four constants namely: A, B_1, B_2, and B_3. We therefore utilize the property of gauge invariance which allows us to set any of the B_i's to zero without any loss of generality [49]. We set $B_1 = 0$, then

$$h_r = -h_\phi \tag{2.7.24}$$

Whence the displacement vector components are

$$u_r = \left[f' + \frac{n}{r} h_z - (ik) h_\phi \right] \cos(n\phi) e^{ikz} \tag{2.7.25}$$

$$u_\phi = \left[-\frac{n}{r} f + (ik) h_r - h_z' \right] \sin(n\phi) e^{ikz} \tag{2.7.26}$$

$$u_z = \left[(ik) f - \frac{(n+1)}{r} h_r - h_r' \right] \cos(n\phi) e^{ikz} \tag{2.7.27}$$

where $'$ denotes differentiation with respect to r.

2.8 Dispersion relations of a clamped cylindrical solid

The frequency equation for the modes of vibration for the cylinder can be obtained by applying the boundary conditions at the surface of the cylinder. If we consider a clamped cylinder at its surface (i.e the cylinder is surrounded by rigid material) then no deformation will be allowed at the surface. Therefore, the components of the displacement vector must vanish at the surface of the cylinder.

If we replace the explicit values of the functions in (2.7.25)-(2.7.27) at $r = a$ and set them to zero, we obtain three equations depending on the constants A, B_2, and B_3. Since these constants are non zero, then the determinant formed by their coefficients must vanish. The determinant set to zero defines the general frequency equation:

$$\begin{vmatrix} \alpha J_{n-1}(\alpha a) - \frac{n}{a} J_n(\alpha a) & ikJ_{n+1}(\beta a) & \frac{n}{a} J_n(\beta a) \\ -\frac{n}{a} J_n(\alpha a) & ikJ_{n+1}(\beta a) & -\beta J_{n-1}(\beta a) + \frac{n}{a} J_n(\beta a) \\ ikJ_n(\alpha a) & -\beta J_n(\beta a) & 0 \end{vmatrix} = 0 \tag{2.8.1}$$

Equation (2.8.1) determines the modes of vibration of a clamped cylinder for all $n \geq 0$. For each n we will have two polarizations; a "longitudinal" polarization and a "transverse" polarization, corresponding to the two terms in the solution (2.7.2).

For $n = 0$ the frequency equation reduces to two factors; one gives the frequency equation for the Torsional modes which are caused by the twisting of the cylinder

about its axis, and the other gives that of the longitudinal modes of vibration which result from extensions and compression of the cylinder along its axis. For $n = 1$ we obtain the ordinary family of flexural modes, and for $n \geq 2$ we obtain the so called flexural modes of circumferential order n. These modes can be described as follows:

1 - The family of torsional modes

The displacement vector for torsional modes in a solid cylinder are described by a single component, namely u_ϕ. This can be obtained from a single potential function H_z given by

$$H_z = B_3 J_0(\beta r) e^{ikz} \tag{2.8.2}$$

From this we find that the only non-zero component of the displacement vector is

$$u_\phi = \beta B_3 J_1(\beta r) e^{ikz} \tag{2.8.3}$$

setting this to zero at $r = a$ we obtain the frequency equation for the torsional modes

$$\beta J_1(\beta a) = 0 \tag{2.8.4}$$

The solutions to this equation are

$$\beta = 0, \quad \text{or} \quad \beta = \frac{z_{1l}}{a} \tag{2.8.5}$$

where z_{1l} is the lth zero of the Bessel functions with $n = 1$.

The first solution gives the bulk dispersion relation which is not physically plausible and thus can be neglected. The second solution on the other hand, results from the presence of the boundary at $r = a$, and hence gives the true dispersion relation of the cylinder. The same frequency equation can be obtained from (2.8.1) by setting $n = 0$.

2 - The family of longitudinal modes

These type of vibration modes occur due to extension or compression of the cylinder along its axis, therefore they result in displacements only along the r and z-directions. The longitudinal modes of a cylinder can thus be described by two components of the displacement vector, u_r and u_ϕ with no dependence on the angular variable ϕ. Taking only ψ and H_ϕ with $n = 0$ yields the following components of the displacement vector:

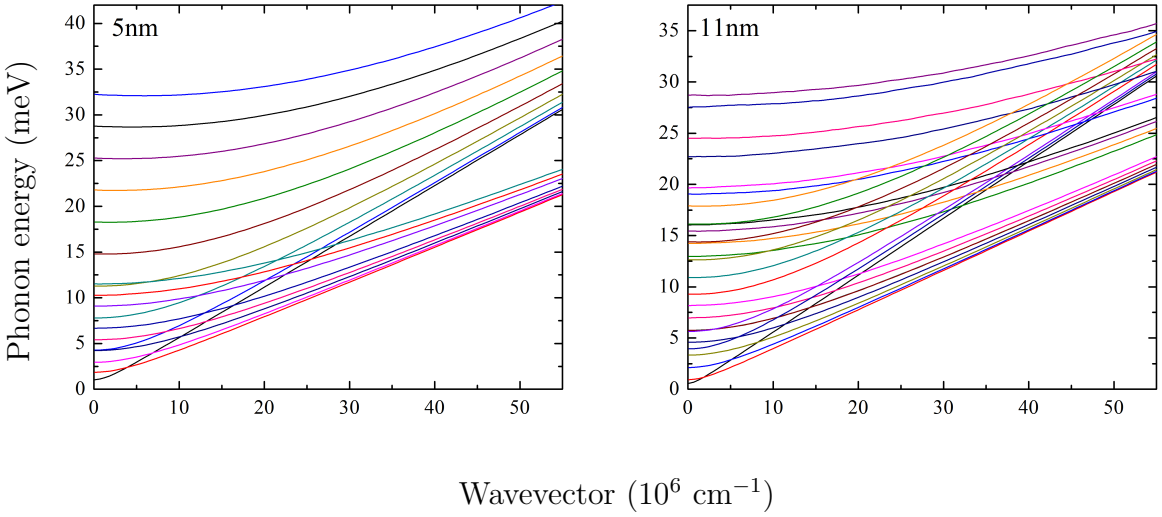

Figure 2.4: Dispersion curves of the longitudinal and torsional vibration modes of clamped NWs of radii 5 and 11 nm obtained by numerically solving (2.8.1) with $n = 0$.

$$u_r = -AJ_1(\alpha r) + (ik)B_2J_1(\beta r) \tag{2.8.6}$$
$$u_z = (ik)AJ_0(\alpha r) - \beta B_2J_0(\beta r) \tag{2.8.7}$$

Evaluating these components at $r = a$ and setting to zero we find

$$\alpha\beta J_0(\beta a)J_1(\alpha a) + k^2J_0(\alpha a)J_1(\beta a) = 0 \tag{2.8.8}$$

This is the dispersion relation for the family of longitudinal modes. Again, this can also be found by setting $n = 0$ in (2.8.1).

By numerically solving (2.8.1) with (2.7.10) and (2.7.14) for $n = 0$ we obtain the dispersion relations of the longitudinal and torsional modes for confined acoustic phonons in single Si NWs. In all numerical calculations of the dispersion curves we use the values: $\rho = 2329Kg/m^3$, $c_l = 8.43 \times 10^3 m/s$, and $c_t = 5.84 \times 10^3 m/s$ which are appropriate for Si. At each k one can find many solutions for α and β, thus the $\omega - k$ diagram will consist of several branches which we may label with an index j, so that $\omega_j(k)$ is the frequency of the jth branch at the mode k.

In Figure 2.4 we show the dispersion relations of the confined longitudinal and torsional acoustic phonon branches in single Si NWs of radii 5nm and 11nm. As can be noticed, the slopes of the confined acoustic phonon branches decrease with

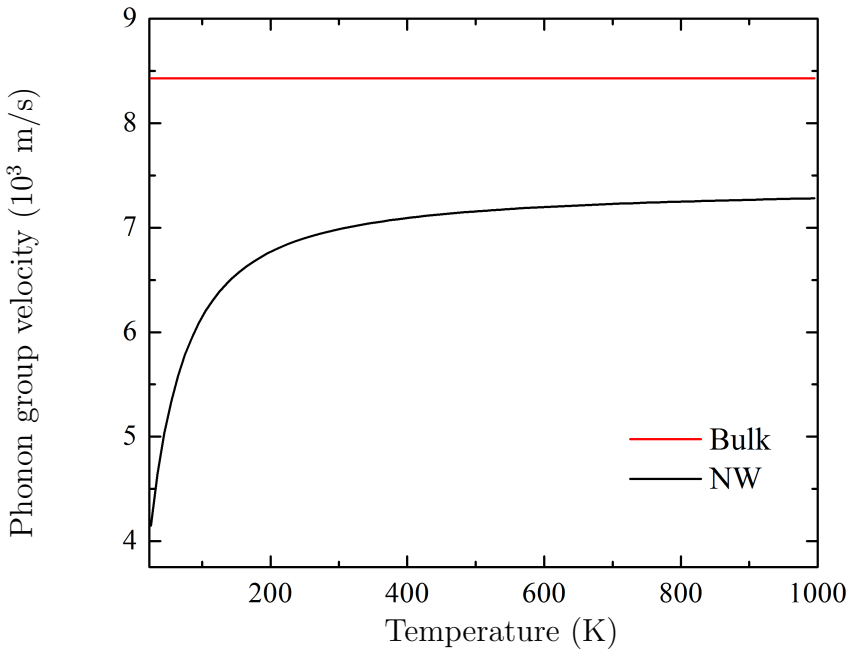

Figure 2.5: Averaged phonon group velocity of the lowest branch of confined phonons in a 5 nm radius NW versus temperature along with the constant bulk longitudinal group velocity.

decreasing wire cross section, which implies a decrease in the averaged phonon group velocities.

The dispersion curves in Figure 2.4 can be used to calculate averaged phonon phase and group velocities. The averaged velocities can be obtained by employing a Boltzmann weights average [50]

$$\overline{v}_j = \frac{\sum_k v_j(k) e^{-\hbar\omega_j(k)/k_B T}}{\sum_k e^{-\hbar\omega_j(k)/k_B T}}, \quad \text{and} \quad \overline{c}_j = \frac{\sum_k c_j(k) e^{-\hbar\omega_j(k)/k_B T}}{\sum_k e^{-\hbar\omega_j(k)/k_B T}} \tag{2.8.9}$$

where

$$v_j(k) = \frac{d\omega_j(k)}{dk}, \quad \text{and} \quad c_j(k) = \frac{\omega_j(k)}{k} \tag{2.8.10}$$

$\overline{v}_j$ is an averaged phonon group velocity of the jth branch, while $\overline{c}_j$ is an averaged phase velocity that approximates the relation between ω and k.

In Figure 2.5 the averaged group velocity of the lowest branch confined phonons based on (2.8.9) is plotted with the bulk group velocity. As can be seen from the figure the group velocity of phonons confined in a NW is much lower than that of their bulk counterparts. In addition, the averaged phonon group velocity found from (2.8.9) is temperature dependent and thus is better suited to describe phonons, which result from atomic vibrations, than the use of a constant group velocity. It is seen that the phonon group velocity in the NW is very small at low temperatures due to the enhancement of the confinement effect in this limit. At higher temperatures the velocity increases since the phonon wavelengths become shorter and thus the boundary effect becomes less important.

3 - The family of flexural modes with $n = 1$

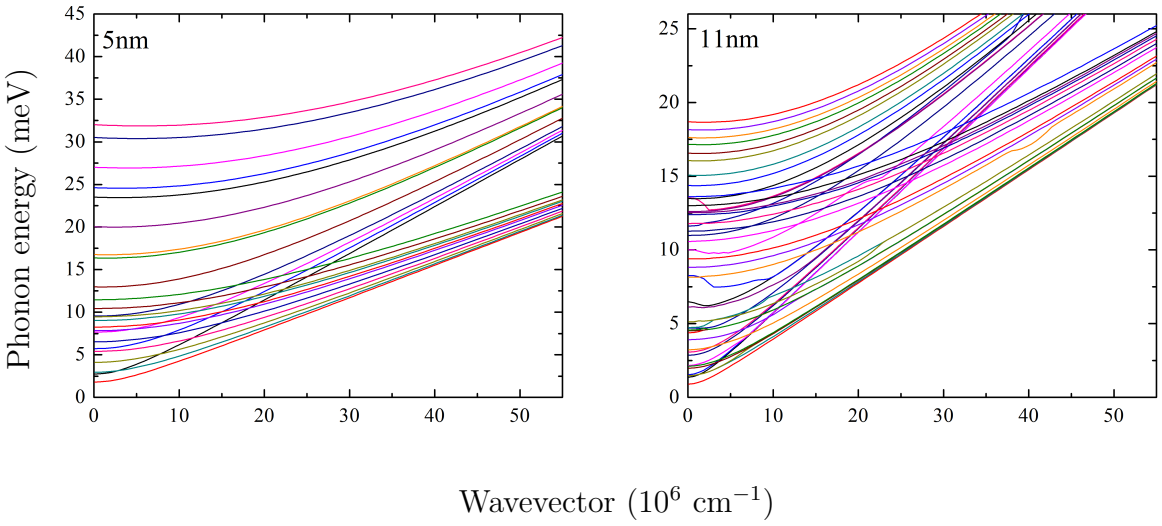

Figure 2.6: Dispersion curves of the flexural modes ($n = 1$) of clamped NWs of radii 5 and 11 nm.

The motion of flexural modes involves all three components of the displacement vector. For $n = 1$ we obtain from (2.8.1) the dispersion relation for the lowest order family of flexural modes:

$$\left(\beta J_0(\beta a) - \frac{1}{a}J_1(\beta a)\right)\left[\beta J_1(\beta a)\left(\alpha J_0(\alpha a) - \frac{1}{a}J_1(\alpha a)\right) - k^2 J_1(\alpha a)J_2(\beta a)\right] - \frac{1}{a}J_1(\beta a)\left[\frac{1}{a}\beta J_1(\alpha a)J_1(\beta a) + k^2 J_2(\beta a)J_1(\alpha a)\right] = 0 \tag{2.8.11}$$

Using the identity

$$J_{n-1}(x) + J_{n+1}(x) = \frac{2n}{x}J_n(x) \tag{2.8.12}$$

The frequency equation for the flexural modes with $n = 1$ can be rewritten as

$$\alpha\beta J_0(\alpha a)J_1(\beta a)\left[(\beta a)J_0(\beta a) - J_1(\beta a)\right] + J_0(\beta a)\left[(\beta a)k^2 J_1(\alpha a)J_0(\beta a) - (\beta^2 + 2k^2)J_1(\alpha a)J_1(\beta a)\right] = 0 \tag{2.8.13}$$

For $n \geq 2$ we obtain higher order flexural modes that are referred to as flexural modes of circumferential order n.

The dispersion curves of the lowest order flexural modes are shown in Figure 2.6 for NWs of radii equal to 5 and 11 nm.

2.9 Dispersion relations of a free surface cylinder

We now consider a cylinder with a free surface (i.e surrounded by vacuum). Since the external stresses are zero the continuity of the stress tensor requires that the stress components vanish at the surface, therefore, the boundary condition at the surface can be written as

$$\sigma_{ik}n_k\Big|_{r=a} = 0 \tag{2.9.1}$$

where $\mathbf{n}$ is a unit vector normal to the surface, and repeated indices are summed over. Since only the r component of $\mathbf{n}$ is non-zero then the boundary condition (2.9.1) reads

$$\sigma_{rr} = \sigma_{r\phi} = \sigma_{rz} = 0, \quad \text{at} \quad r = a \tag{2.9.2}$$

The components of the stress tensor can be found from the strain components using (2.6.1). From (2.5.3) it is easily seen that u_{ii} is just the divergence of the displacement vector.

Whence, the stress components normal to the surface are

$$\sigma_{rr} = \lambda\nabla^2\psi + 2\mu u_{rr} \tag{2.9.3}$$
$$\sigma_{r\phi} = 2\mu u_{r\phi} \tag{2.9.4}$$
$$\sigma_{rz} = 2\mu u_{rz} \tag{2.9.5}$$

The first term in σ_{rr} only involves the potential function ψ since the divergence of the second term in (2.7.2) vanishes, and using (2.7.3) we find $\nabla^2\psi = -(\alpha^2+k^2)\psi$.

In cylindrical coordinates the strain tensor components are given by

$$u_{rr} = \frac{\partial u_r}{\partial r} \tag{2.9.6}$$
$$u_{r\phi} = \frac{1}{2}\left[\frac{\partial u_\phi}{\partial r} - \frac{u_\phi}{r} + \frac{1}{r}\frac{\partial u_r}{\partial \phi}\right] \tag{2.9.7}$$
$$u_{rz} = \frac{1}{2}\left[\frac{\partial u_r}{\partial z} + \frac{\partial u_z}{\partial r}\right] \tag{2.9.8}$$

Inserting these expressions in (2.9.3)-(2.9.5) and making use of (2.7.11), (2.7.13), and (2.7.16) along with some juggling we find

$$\sigma_{rr} = \left[\left(2\mu f'' - \lambda(\alpha^2+k^2)f\right) + 2\mu\frac{n}{r}\left(h_z' - \frac{1}{r}h_z\right) + 2\mu(ik)h_r'\right]\cos(n\phi)e^{ikz} \tag{2.9.9}$$

$$\sigma_{r\phi} = \mu\left[-\frac{2n}{r}\left(f' - \frac{1}{r}f\right) + ik\left(h_r' - \frac{(n+1)}{r}h_r\right) - (2h_z'' + \beta^2 h_z)\right]\sin(n\phi)e^{ikz} \tag{2.9.10}$$

$$\sigma_{rz} = \mu\left[2ikf' + ik\frac{n}{r}h_z - \left(k^2 - \beta^2 + \frac{n(n+1)}{r^2}\right)h_r - \frac{n}{r}h_r'\right]\cos(n\phi)e^{ikz} \tag{2.9.11}$$

Evaluating these expressions at $r = a$ and setting to zero gives the general frequency equation for all possible modes of vibration of the free surface cylinder, which is given on he following page:

$$\begin{vmatrix} (\alpha a)J_{n-1}(\alpha a) + \left[(\alpha a)^2 - n(n+1) + \dfrac{\lambda a^2(\alpha^2+k^2)}{2\mu}\right]J_n(\alpha a) & ik\left[a(n+1)J_{n+1}(\beta a) - \beta a^2 J_n(\beta a)\right] & n\left[(n+1)J_n(\beta a) - (\beta a)J_{n-1}(\beta a)\right] \\ -2n\left[(\alpha a)J_{n-1}(\alpha a) - (n+1)J_n(\alpha a)\right] & ik\left[\beta a^2 J_n(\beta a) - 2a(n+1)J_{n+1}(\beta a)\right] & \left[2(\beta a)J_{n-1}(\beta a) + \big((\beta a)^2 - 2n(n+1)\big)J_n(\beta a)\right] \\ 2ik\alpha\left[a^2 J_{n-1}(\alpha a) - naJ_n(\alpha)\right] & -\left[a^2(k^2-\beta^2)J_{n+1}(\beta a) + n(\beta a)J_n(\beta a)\right] & (ik)naJ_n(\beta a) \end{vmatrix} = 0 \quad (2.9.12)$$

Therefore, for the free surface cylinder we have the following modes of vibration:

1 - The family of torsional modes

Considering only the potential function (2.8.2) we find the following frequency equation for the torsional modes of vibration of a free surface cylinder

$$\beta\Big[2J_1(\beta a) - (\beta a)J_0(\beta a)\Big] = 0 \tag{2.9.13}$$

This has two solutions

$$\beta = 0, \quad \text{or} \quad 2J_1(\beta a) = (\beta a)J_0(\beta a) \tag{2.9.14}$$

Again we obtain the non-physical bulk solution along with the actual solution given by the second equation in (2.9.14). As mentioned earlier this can also be obtained from the general frequency equation (2.9.12) by setting $n = 0$.

2 - The family of longitudinal modes

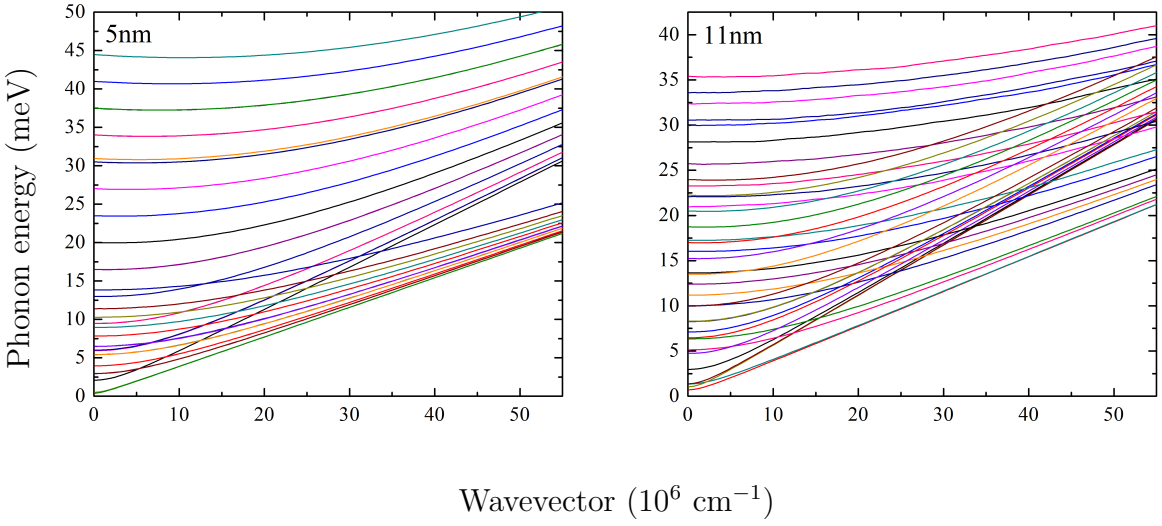

Figure 2.7: Dispersion curves of the longitudinal and torsional vibration modes ($n = 0$) of free surface NWs of radii 5 an 11 nm.

The family of longitudinal modes is obtained from the potential functions ψ and H_ϕ with $n = 0$. Using these to evaluate the expressions of the stress components at $r = a$ and setting equal to zero we find the frequency equation for the longitudinal modes:

$$\frac{2\alpha}{a}(\beta^2+k^2)J_1(\beta a)J_1(\alpha a) - J_0(\alpha a)J_1(\beta a)\left[2(\beta^2-k^2)\left(\alpha^2+\frac{\lambda}{2\mu}(\alpha^2+k^2)\right)\right] - 4k^2\alpha\beta J_1(\alpha a)J_0(\beta a) = 0 \quad (2.9.15)$$

One can easily check that (2.9.12) with $n = 0$ yields the same dispersion relation for the longitudinal modes.

3 - The family of flexural modes

Equation (2.9.12) with $n \geq 1$ provides the dispersion relations of the flexural modes of order n as discussed for the clamped cylinder.

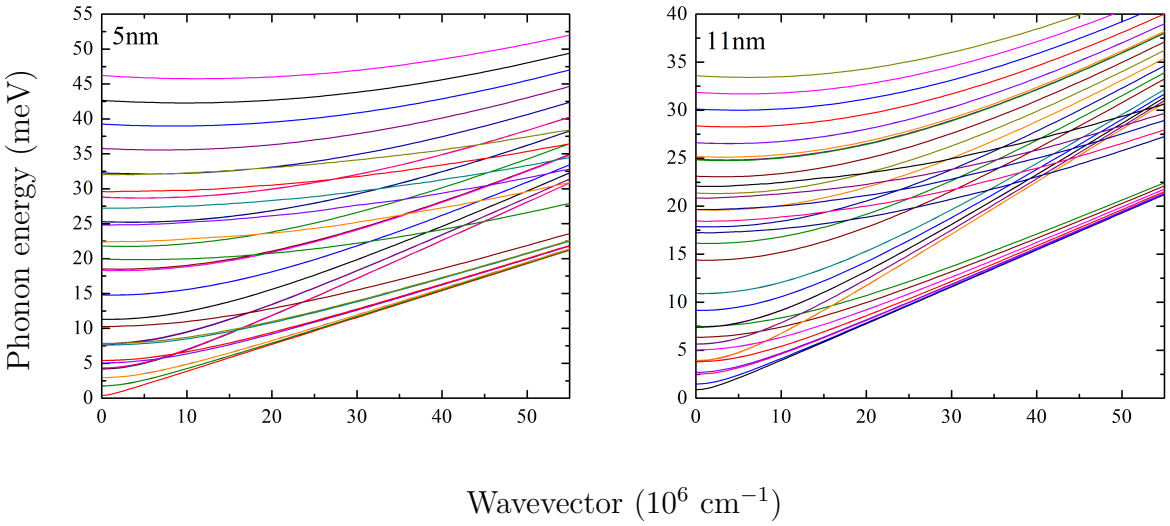

Figure 2.8: Dispersion curves of the flexural modes ($n = 1$) of free surface NWs of radii 5 and 11 nm.

The dispersion curves of flexural vibration modes of a free surface cylinder are shown in Figure 2.8.

2.10 Waveveccctor components in cylindrical coordinates

In order to obtain the wavevector components for a cylinder the wave equation $\nabla^2 U + k^2 U$ must be solved in cylindrical coordinates (r, ϕ, z):

$$\frac{1}{r}\frac{\partial}{\partial r}\left(r\frac{\partial U}{\partial r}\right)+\frac{1}{r^2}\frac{^2U}{\partial\phi^2}+\frac{\partial^2 U}{\partial z^2}+k^2U=0 \tag{2.10.1}$$

We use the following separation of variable

$$U(r,\phi,z)=R(r)\Phi(\phi)Z(z) \tag{2.10.2}$$

Replacing this in (2.10.1) we obtain

$$\begin{aligned}&\frac{1}{rR(r)}\frac{d}{dr}\left(r\frac{dR(r)}{dr}\right)+\frac{1}{r^2\Phi(\phi)}\frac{d^2\Phi(\phi)}{d\phi^2}+\frac{d^2Z(z)}{dz^2}+k^2=0\\ \Rightarrow\ &\frac{1}{rR(r)}\frac{d}{dr}\left(r\frac{dR(r)}{dr}\right)+\frac{1}{r^2\Phi(\phi)}\frac{d^2\Phi(\phi)}{d\phi^2}+k^2=-\frac{1}{Z(z)}\frac{d^2Z(z)}{dz^2}=k_z^2\end{aligned} \tag{2.10.3}$$

where, k_z is a constant.

The solution to the differential equation given by the last equality in (2.10.3) can be written in the form

$$Z(z)=e^{ik_z z} \tag{2.10.4}$$

We can now rewrite (2.10.3) in the following way

$$\frac{r}{R(r)}\frac{d}{dr}\left(r\frac{dR(r)}{dr}\right)(k^2-k_z^2)r^2=-\frac{1}{\Phi(\phi)}\frac{d^2\Phi(\phi)}{d\phi^2}=n^2 \tag{2.10.5}$$

where, n is an integer.

We define the wavevector components k_r such that

$$k^2=k_r^2+k_z^2 \tag{2.10.6}$$

thus (2.10.5) gives the following two differential equations

$$\frac{d^2\Phi(\phi)}{d\phi^2}+n^2\Phi(\phi)=0 \tag{2.10.7}$$

$$r^2\frac{d^2R(r)}{dr^2}+r\frac{dR(r)}{dr}+(k_r^2r^2-n^2)R(r)=0 \tag{2.10.8}$$

The solution to the first is simply

$$\Phi(\phi)=e^{\pm in\phi} \tag{2.10.9}$$

For the second we make the change of variable $\rho_r=k_r r$ so that it can be written as

$$\rho_r^2 \frac{d^2R(\rho_r)}{d\rho_r^2} + \rho_r \frac{dR(\rho_r)}{d\rho_r} + \left(\rho_r^2 - n^2\right) R(\rho_r) = 0 \tag{2.10.10}$$

This is Bessel's equation whose solutions are the Bessel functions $J_n(k_r r)$. We exclude Bessel functions of the second kind since they are not finite at $r = 0$. Thus the most general solution of the wave equation is

$$U_n(r, \phi, z, t) = \sum_n J_n(k_r r) e^{ik_z z} e^{\pm in\phi} e^{-i\omega t} \tag{2.10.11}$$

By applying the boundary conditions at the surface of the rod we may obtain the wavevector components. For a clamped surface we use the Dirichlet boundary condition

$$U(r = a) = 0 \tag{2.10.12}$$

This requires

$$J_n(k_r a) = 0 \tag{2.10.13}$$

Hence,

$$k_r = \frac{z_{ln}}{a} \tag{2.10.14}$$

where z_{ln} is the lth zero of the Bessel function of order n.

For a free surface rod we utilize the Neumann boundary condtion i.e

$$\frac{\partial U}{\partial r}\Big|_{r=a} = 0 \tag{2.10.15}$$

So that

$$J_n^{'}(k_r a) = 0 \tag{2.10.16}$$

where $'$ denotes the derivative with respect to the argument.

Therefore, in this case we have

$$k_r = \frac{z_{ln}^{'}}{a} \tag{2.10.17}$$

where $z_{ln}^{'}$ are the zeros of the derivatives of the Bessel functions.

Chapter 3

The Boltzmann transport equation

The phonon distribution function is required for the calculation of thermal properties in solids. At equilibrium the phonon distribution function is given by the Bose-Einstein distribution function which depends only on energy and temperature. Transport phenomena, however, occur only when the system is out of equilibrium. Therefore, the calculation of thermal currents and thermal conductivity, for instance, requires knowledge of a non-equilibrium distribution function. In this chapter we introduce non-equilibrium distribution functions based on the Liouville equation and the simpler Boltzmann equation, and we derive a solution for the phonon Boltzmann equation in the cylindrical geometry.

3.1 The phase space and Liouville's equation

Consider a system with N particles which are described by the generalized coordinate $\mathbf{r}$ and the generalized momentum $\mathbf{p}$. If we assume that there are m degrees of freedom, i.e there are m generalized coordinates, and m generalized momenta, the number of degrees of freedom of the entire system is $2n = 2m \times N$. These $2n$ variables form a $2n$-dimensional space called a phase space. The system at any instant can be described as one point in such a space. The time evolution of the system traces one line in such a $2n$-dimensional phase space, called a flow line.

Now we consider an ensemble of systems satisfying the same macroscopic constraints. From classical mechanics we know that for given initial conditions the trajectory of the system is uniquely determined. Since the initial conditions for each system differ from that of other systems in the ensemble, the traces of systems in such an ensemble do not intersect, i.e the flow lines in phase space do not intersect.

The number of systems in an ensemble is very large, much larger than the number of particles in one system. As a result, we can treat the points of the ensemble, each representing a microstate of the original macroscopic system, as forming a continuum in the phase space. We can therefore, define a particle density function $f^{(N)}$ such that the number of systems in the neighborhood of any point $(\mathbf{r}^{(n)}, \mathbf{p}^{(n)})$ in the phase space, where $\mathbf{r}^{(n)} = (\mathbf{r}_1, \mathbf{r}_2, ..., \mathbf{r}_N) = (r^1, r^2, ..., r^n)$ are all the space coordinates of the N particles and similarly $\mathbf{p}^{(n)}$ represents the momenta coordinates, is given by

$$f^{(N)}(t, \mathbf{r}^{(n)}, \mathbf{p}^{(n)})\Delta\mathbf{r}^{(n)}\Delta\mathbf{p}^{(n)} \tag{3.1.1}$$

in a small volume $\Delta\mathbf{r}^{(n)}\Delta\mathbf{p}^{(n)} = (\Delta\mathbf{r}_1\Delta\mathbf{r}_2...\Delta\mathbf{r}_N)(\Delta\mathbf{p}_1\Delta\mathbf{p}_2...\Delta\mathbf{p}_N)$ in the phase space.

The particle density in the phase space $f^{(N)}(t, \mathbf{r}^{(n)}, \mathbf{p}^{(n)})$ is called the N-particle distribution function, which represents the probability of finding a particular system at a specific state defined by $\mathbf{r}^{(n)}$ and $\mathbf{p}^{(n)}$.

The time evolution of the N-particle distribution function is given by Liouville's equation. The rate of change of the distribution function is related to its Poisson bracket with the system Hamiltonian $H^{(N)}(t, \mathbf{r}^{(n)}, \mathbf{p}^{(n)})$

$$\begin{aligned}\frac{\partial f^{(N)}}{\partial t} &= -\left\{f^{(N)}, H^{(N)}\right\} \\ &= -\left[\sum_{i=1}^{n} \frac{\partial f^{(N)}}{\partial r^{(i)}}\frac{\partial H^{(N)}}{\partial p^{(i)}} - \sum_{i=1}^{n} \frac{\partial f^{(N)}}{\partial p^{(i)}}\frac{\partial H^{(N)}}{\partial r^{(i)}}\right]\end{aligned} \tag{3.1.2}$$

Using Hamilton's equations (3.1.2) can be written as

$$\frac{\partial f^{(N)}}{\partial t} = -\left[\sum_{i=1}^{n} \frac{\partial f^{(N)}}{\partial r^{(i)}}\frac{\partial p^{(i)}}{\partial t} + \sum_{i=1}^{n} \frac{\partial f^{(N)}}{\partial p^{(i)}}\frac{\partial r^{(i)}}{\partial t}\right] \tag{3.1.3}$$

Equation (3.1.3) is the Liouville equation that governs the time evolution of the N-particle distribution function $f^{(N)}$. Direct solution of (3.1.3) is impossible, however, due to the large number of variables involved, which is on the order of Avogadro's number. In addition, solving the Liouville equation requires the determination of the exact initial conditions of the ensemble. Therefore, a simpler approach based on the Boltzmann equation must be adopted as in the next section.

3.2 The phonon Boltzmann equation

One way to simplify Liouville's equation is to consider one particle in a system. This is a representative particle having coordinate $\mathbf{r}_1$ and momentum $\mathbf{p}_1$; each having m components. We introduce a one particle distribution function $f^{(1)}(t, \mathbf{r}_1, \mathbf{p}_1)$ by averaging the N-particle distribution function over the rest of the $(N-1)$ particles in the system

$$f^{(1)}(t, \mathbf{r}_1, \mathbf{p}_1) = \frac{N!}{(N-1)!} \int f^{(N)}(t, \mathbf{r}^n, \mathbf{p}^n) d\mathbf{r}_1 d\mathbf{r}_2 ... d\mathbf{r}_N d\mathbf{p}_1 d\mathbf{p}_2 ... d\mathbf{p}_N \qquad (3.2.1)$$

where $n = m \times N$ and the factorials are normalization factors. For brevity the subscript 1 will be dropped and henceforth we will use $(\mathbf{r}, \mathbf{p})$ as the coordinates and momenta of the particle.

Since $f^{(N)}(t, \mathbf{r}^{(n)}, \mathbf{p}^{(n)})$ represents the number density of systems having generalized coordinates $(\mathbf{r}^{(n)}, \mathbf{p}^{(n)})$ in the ensemble, the one particle distribution function represents the number density of systems having $(\mathbf{r}, \mathbf{p})$, so that $f(t, \mathbf{r}, \mathbf{p}) d^3\mathbf{r} d^3\mathbf{p}$ gives the number of systems in $d^3\mathbf{r} d^3\mathbf{p}$.

The use of the one particle distribution function results in a significant reduction of the number of variables. For one mole of a monatomic gas with 6×10^{23} atoms, for example, the number of variables in the phase space is $6 \times 6 \times 10^{23}$, because we have three spatial coordinates and three momentum coordinates. On the other hand, the one particle phase space for monatomic atoms has only three spatial coordinates and three momentum coordinates. Carrying out the averaging method to obtain the one particle distribution function on the the Liouville equation (3.1.3) we find

$$\frac{\partial f}{\partial t} + \frac{d\mathbf{r}}{dt} . \nabla_{\mathbf{r}} f + \frac{d\mathbf{p}}{dt} . \nabla_{\mathbf{p}} f = \frac{\partial f}{\partial t}\Big|_{scatt} \qquad (3.2.2)$$

where $\nabla_{\mathbf{r}}$ and $\nabla_{\mathbf{p}}$ are the position and momentum gradients respectively.

Unlike the $2n$-phase space for the Liouville equation, in which one point represents a system and the flow lines of the points do not intersect, the particle represented by f interacts with other particles in the system. The right-hand side of (3.2.2) lumps the interaction of this one particle with the other particles in the system and represents the non-conserving nature of the one particle distribution function. This scattering term represents the net rate of gaining particles at point $(\mathbf{r}, \mathbf{p})$ and should not be thought of as a simple partial derivative. Further details about the scattering term are presented in section 3.3. Equation (3.2.2) is called the Boltzmann equation or the Boltzmann transport equation.

It can be seen that the second term on the left-hand side of (3.2.2) gives the rate of change of the distribution function due to diffusion, while the last term on the left-hand side is a force term giving the rate of change of the distribution due to external forces. Alternatively, the Boltzmann equation can be rewritten using the velocity $\mathbf{v} = \mathbf{p}/m$ or the wavevector $\mathbf{k} = \mathbf{p}/\hbar$ of the particle

$$\frac{\partial f}{\partial t} + \mathbf{v}.\nabla_{\mathbf{r}} f + \frac{\mathbf{F}}{m}.\nabla_{\mathbf{v}} f = \frac{\partial f}{\partial t}\Big|_{scatt} \tag{3.2.3}$$

$$\frac{\partial f}{\partial t} + \mathbf{v}.\nabla_{\mathbf{r}} f + \frac{\mathbf{F}}{\hbar}.\nabla_{\mathbf{k}} f = \frac{\partial f}{\partial t}\Big|_{scatt} \tag{3.2.4}$$

The use of $\hbar$ in (3.2.4) implies that the Boltzmann equation may be applied to quantum particles as long as we do not consider the phase coherence of the particles.

For phonons the time evolution of the one particle phonon distribution function denoted $N_{\mathbf{k}s}$, where s is the phonon polarization, is given by (3.2.4) with $\mathbf{F} = 0$, since phonons are not affected by external forces. Moreover, in the steady state of heat flow (3.2.4) leads to the phonon Boltzmann equation

$$-\mathbf{v}_s.\nabla N_{\mathbf{k}s} + \frac{\partial N_{\mathbf{k}s}}{\partial t}\Big|_{scatt} = 0 \tag{3.2.5}$$

It should be understood that the velocity in (3.2.5) is the phonon group velocity.

The distribution function obtained from the Boltzmann equation may be used for the calculation of averaged quantities, such as average energy and thermal current. Once the distribution function is known we can calculate the volume average of any microscopic quantity of the particle from

$$\big\langle X(\mathbf{r})\big\rangle = \frac{1}{V}\sum_{\mathbf{k}s} X(\mathbf{r},\mathbf{k}s)N_{\mathbf{k}s} = \frac{1}{(2\pi)^3}\int X(\mathbf{r},\mathbf{k}s)N_{\mathbf{k}s}d^3\mathbf{k} \tag{3.2.6}$$

The summation over the wavevectors is changed into integration by noting that the volume of one quantum state in k-space is $V/(2\pi)^3$.

3.3 Scattering integral and the relaxation time approximation

In order to find the scattering term in (3.2.5) we consider the collision process between two particles. The collision will be a time dependent process, thus we can treat the collision by considering the time dependent interaction between the two particles as a perturbation $H^{'}(\mathbf{r},t)$ from the equilibrium steady state

non interacting energy H_0. Using the perturbation method we can calculate the probability for the system to transition from one quantum state Ψ_i to another Ψ_f, the transition rate is given by

$$\begin{aligned} P_i^f &= \frac{2\pi}{\hbar}\left|\int \Psi_f^* H^{'} \Psi_i d^3\mathbf{r}\right|^2 \delta(E_f - E_i) \\ &= \frac{2\pi}{\hbar} M_{if}^2 \delta(E_f - E_i) \end{aligned} \tag{3.3.1}$$

where,

$$M_{if} = (\Psi_i, H^{'}\Psi_f) = \int \Psi_f^* H^{'} \Psi_i d^3\mathbf{r} \tag{3.3.2}$$

is the scattering matrix.

(3.3.1) is often referred to as Fermi's golden rule which gives the transition rate from one set of quantum states of the two particles into another set due to scattering. The scattering term in the Boltzmann equation is the net gain of particles in one quantum state. Then, for the two particle system if the initial wave vector of one particle is $\mathbf{k}$ and it collides with another of wave vector $\mathbf{k}^{'}$, with the momenta of the two particles after collision being $\mathbf{k}^{''}$ and $\mathbf{k}^{'''}$, then the scattering term for the particle at state $\mathbf{k}$ is expressed as

$$\frac{\partial N_{\mathbf{k}s}}{\partial t}\Big|_{scatt} = \sum_{\mathbf{k}'s'} \sum_{\mathbf{k}''s''} \sum_{\mathbf{k}'''s'''} \left[P^{\mathbf{k}s,\mathbf{k}'s'}_{\mathbf{k}''\mathbf{s}'',\mathbf{k}'''s'''} - P^{\mathbf{k}''\mathbf{s}'',\mathbf{k}'''s'''}_{\mathbf{k}s,\mathbf{k}'s'} \right] \tag{3.3.3}$$

Using the conservation of energy and momentum

$$E(\mathbf{k}s) + E(\mathbf{k}^{'}s^{'}) = E(\mathbf{k}^{''}s^{''}) + E(\mathbf{k}^{'''}s^{'''}), \quad \mathbf{k} + \mathbf{k}^{'} = \mathbf{k}^{''} + \mathbf{k}^{'''} \tag{3.3.4}$$

the transition rates can be written as

$$P^{\mathbf{k}s,\mathbf{k}'s'}_{\mathbf{k}''\mathbf{s}'',\mathbf{k}'''s'''} = N_{\mathbf{k}s} N_{\mathbf{k}'s'} (N_{\mathbf{k}''s''} + 1)(N_{\mathbf{k}'''s'''} + 1) W(\mathbf{k}s, \mathbf{k}^{'}s^{'} \longrightarrow \mathbf{k}^{''}s^{''}, \mathbf{k}^{'''}s^{'''}) \tag{3.3.5}$$

$$P^{\mathbf{k}''\mathbf{s}'',\mathbf{k}'''s'''}_{\mathbf{k}s,\mathbf{k}'s'} = N_{\mathbf{k}''s''} N_{\mathbf{k}'''s'''} (N_{\mathbf{k}s} + 1)(N_{\mathbf{k}'s'} + 1) W(\mathbf{k}^{''}s^{''}, \mathbf{k}^{'''}s^{'''} \longrightarrow \mathbf{k}s, \mathbf{k}^{'}s^{'}) \tag{3.3.6}$$

where $W(\mathbf{k}s, \mathbf{k}^{'}s^{'} \longrightarrow \mathbf{k}^{''}s^{''}, \mathbf{k}^{'''}s^{'''})$ is the intrinsic transition probability (which is independent of phonon distribution) between the initial and final states.

Using the principle of detailed balance, which states that the transition probability is the same in the forward and backward direction we can write the scattering term (3.3.3) as

$$\frac{\partial N_{\mathbf{k}}}{\partial t}\Big|_{scatt} = \sum_{\mathbf{k}'s'}\sum_{\mathbf{k}''s''}\sum_{\mathbf{k}'''s'''}\big[N_{\mathbf{k}s}N_{\mathbf{k}'s'}(N_{\mathbf{k}''s''}+1)(N_{\mathbf{k}'''}+1) - N_{\mathbf{k}''s''}N_{\mathbf{k}'''s'''}(N_{\mathbf{k}s}+1)(N_{\mathbf{k}'s'}+1)\big]W(\mathbf{k}s,\mathbf{k}'s' \longrightarrow \mathbf{k}''s'',\mathbf{k}'''s''') \tag{3.3.7}$$

We can change from summation over the wave vectors into integration using the rule

$$\sum_{\mathbf{k}} \longrightarrow \frac{V}{(2\pi)^3}\int d^3\mathbf{k} \tag{3.3.8}$$

where V is the volume of the crystal. Then we have

$$\frac{\partial N_{\mathbf{k}}}{\partial t}\Big|_{scatt} = \frac{V^3}{(2\pi)^9}\int \big[N_{\mathbf{k}s}N_{\mathbf{k}'s'}(N_{\mathbf{k}''s''}+1)(N_{\mathbf{k}'''s'''}+1) - N_{\mathbf{k}''s''}N_{\mathbf{k}'''s'''}(N_{\mathbf{k}s}+1)(N_{\mathbf{k}'s'}+1)\big]W(\mathbf{k},\mathbf{k}' \longrightarrow \mathbf{k}'',\mathbf{k}''')d^3\mathbf{k}'d^3\mathbf{k}''d^3\mathbf{k}''' \tag{3.3.9}$$

Inserting this in (3.2.5) the Boltzmann equation assumes the form

$$v_s(\mathbf{k}).\nabla N_{\mathbf{k}s} = \frac{V^3}{(2\pi)^9}\int \big[N_{\mathbf{k}s}N_{\mathbf{k}'s'}(N_{\mathbf{k}''s''}+1)(N_{\mathbf{k}'''s'''}+1) - N_{\mathbf{k}''s''}N_{\mathbf{k}'''s'''}(N_{\mathbf{k}s}+1)(N_{\mathbf{k}'s'}+1)\big]W(\mathbf{k},\mathbf{k}' \longrightarrow \mathbf{k}'',\mathbf{k}''')d^3\mathbf{k}'d^3\mathbf{k}''d^3\mathbf{k}''' \tag{3.3.10}$$

The Boltzmann equation written in this form is a complicated integro-differential equation which is excessively difficult to solve. In order to solve (3.3.10) we approximate the scattering term by the relaxation time approximation

$$\frac{\partial N_{\mathbf{k}s}}{\partial t}\Big|_{scatt} \approx -\frac{N-\overline{N}}{\tau(\mathbf{r},\mathbf{k})} \tag{3.3.11}$$

where $\tau(\mathbf{r},\mathbf{k})$ is a relaxation time, which is the time needed to relax the non-equilibrium system back to the equilibrium distribution.

The scattering of the carriers can be due to many processes that may coexist, each having its own relaxation time. The total relaxation time can be obtained from the individual relaxation times τ_i according to the Matthiessen rule

$$\frac{1}{\tau} = \sum_i \frac{1}{\tau_i} \tag{3.3.12}$$

Therefore under the relaxation time approximation, the Boltzmann equation takes the form

$$-\mathbf{v}_s(\mathbf{k}).\nabla N_{\mathbf{k}s} + \frac{\overline{N} - N}{\tau(\mathbf{r}, \mathbf{k})} = 0 \tag{3.3.13}$$

3.4 Solution of the phonon Boltzmann equation for bulk materials

We consider a bulk or infinite material with a temperature gradient applied across it. The temperature gradient will cause the phonons in the material to be deviated from their equilibrium distribution so that they conduct heat along its direction. If we assume that the temperature gradient is weak so that the deviation from equilibrium is small then we can consider a solution to the Boltzmann equation of the form (2.3.3).

Since the dimensions of the material extend to infinity the phonon distribution function will not have any appreciable deviation due to spatial variation, however it will have an implicit dependence on position through the spatially variable temperature. As a result, we have

$$-\mathbf{v}.\nabla N \approx -\mathbf{v}.\nabla T \frac{d\overline{N}}{dT} \tag{3.4.1}$$

Where ∇T is the applied temperature gradient.

Under the relaxation time approximation the phonon deviation distribution function for bulk materials can then be immediately read off from the Boltzmann equation (3.3.13)

$$\widetilde{N} = R\tau \tag{3.4.2}$$

where we defined $R = -\mathbf{v}.\nabla T \frac{d\overline{N}}{dT}$ and τ is the total relaxation time obtained from (3.3.12).

Thus, for bulk materials we have

$$\widetilde{N} = -\mathbf{v}.\nabla T \frac{\hbar\omega}{k_B T^2} \frac{e^{\hbar\omega/k_B T}}{(e^{\hbar\omega/k_B T} - 1)^2} \tau \tag{3.4.3}$$

3.5 Solution of the the Boltzmann equation in rectangular coordinates

A distribution function appropriate for thin films or rods with square cross-section can be obtained by solving the phonon Boltzmann equation in rectangular coordinates. We consider that a temperature gradient is applied along the z-direction and the length of the film or rod is assumed to be very large along the direction of the temperature gradient. Since the rod or film extends to infinity along the direction of the temperature gradient the variation of the deviated distribution function along that direction can be neglected . Thus if v_x, v_y, and v_z are the components of the phonon group velocity along the x, y, and z directions respectively, the Boltzmann equation assumes the form

$$v_x \frac{\partial \widetilde{N}}{\partial x} + v_y \frac{\partial \widetilde{N}}{\partial y} + v_z \frac{\partial T}{\partial z} \frac{d\overline{N}}{dT} + \frac{\widetilde{N}}{\tau} = 0 \tag{3.5.1}$$

This can be rewritten as

$$v_x \frac{\partial \widetilde{N}'}{\partial x} + v_y \frac{\partial \widetilde{N}'}{\partial y} + \frac{\widetilde{N}'}{\tau} = 0 \tag{3.5.2}$$

where $\widetilde{N} = \widetilde{N}' + R\tau$.

The subsidiary equations for solving (3.5.2) are

$$\frac{dx}{v_x} = \frac{dy}{v_y} = -\tau \frac{d\widetilde{N}'}{\widetilde{N}'} \tag{3.5.3}$$

of which two independent solutions are

$$\frac{x}{v_x} - \frac{y}{v_y} = \text{constant}, \quad \text{and} \quad \widetilde{N}' e^{x/\tau v_x} = \text{constant} \tag{3.5.4}$$

thus the general solution of (3.5.2) is

$$\widetilde{N}' = e^{-x/\tau v_x} \phi\left(\frac{x}{v_x} - \frac{y}{v_y}\right) = \exp\left\{ -\frac{1}{\tau}\left[\frac{x}{v_x} + \psi\left(\frac{x}{v_x} - \frac{y}{v_y}\right)\right]\right\} \tag{3.5.5}$$

where ϕ and ψ are arbitrary functions of the velocities v_x and v_y.

3.6 Solution of the phonon Boltzmann equation in cylindrical coordinates

Let us consider a cylinder of radius a directed along the z-axis. In order to evaluate the phonon deviation in this geometry the Boltzmann equation must be

solved in cylindrical coordinates (r, ϕ, z). Let $\mathbf{v} = (v_r, v_\phi, v_z)$ be the total phonon group velocity, where v_r, v_ϕ, and v_z are its components along the radial, Azimuthal and z-directions respectively. The length of the cylinder is taken to be much larger than its radius so that the cylinder can effectively be considered infinite in the z-direction. A constant temperature gradient is applied along the axis of the cylinder. The phonon distribution function can then be taken independent of the angular variable ϕ due to the symmetry of the cylindrical rod, but will depend on r and z due to the presence of the boundary and the applied temperature gradient. Moreover, if we consider that the temperature gradient is too weak to significantly displace the distribution function, the Boltzmann equation (3.3.13) in cylindrical coordinates takes the form

$$\frac{\partial \widetilde{N}'}{\partial r} + \frac{\widetilde{N}'}{\tau v_r} = 0 \tag{3.6.1}$$

where again $\widetilde{N} = \widetilde{N}' + R\tau$.

Whence, the phonon deviation can be written as

$$\widetilde{N} = R\tau \left[1 + G(v_r) e^{-r/\tau v_r} \right] \tag{3.6.2}$$

In which G is an arbitrary function of the phonon radial velocity, to be determined by the boundary conditions.

Let G_+ be the value of G for positive values of v_r and G_- for negative values. A phonon approaching the axis of the cylinder will undergo a change of sign in its radial velocity at $r = 0$. However, this change in sign in not physical but rather a result of our convention for the sign of the velocity. Thus, we must have $G_+ = G_-$. This can be satisfied if G is a function of the absolute value of v_r i.e $G(|v_r|)$.

A phonon reaching the boundary of the cylinder can either be reflected or diffuse in a random direction depending on the surface roughness. A uniformly polished (or smooth) surface will specularly reflect (elastically scatter) all phonons incident upon it, whereas a completely rough surface will cause the phonons to diffuse (inelastically scatter) in random directions. In the intermediate case i.e when the boundary is partially elastic and partially inelastic, the effect of the boundary can be studied with the help of a specularity parameter p which gives the fraction of phonons that are specularly reflected by the boundary and is related to the surface roughness.

An approximate expression for the specularity parameter has been given by Ziman [19]

$$p = e^{-16\pi\eta^2/\lambda^2} \tag{3.6.3}$$

where η is the mean surface roughness and λ is the wavelength of the plane wave normally incident to the surface.

Expression (3.6.3) was obtained by employing a treatment analogous to that of the scattering of electromagnetic radiation by a rough surface.

Since an elastic scattering is just a reflection at the surface then if a phonon approaches the boundary with velocity v_r it will be reflected with velocity $-v_r$ at the surface. On the other hand, inelastically scattered phonons will defuse in random directions, which will cause them to lose their drift velocity and so that their distribution function will be given by the equilibrium distribution function, and therefore they will not contribute to the thermal current. Hence, the boundary condition at $r = a$ can be written as follows

$$\overline{N} + \widetilde{N}(r = a, -v_r) = p\big[\overline{N} + \widetilde{N}(r = a, v_r)\big] + (1 - p)\overline{N} \tag{3.6.4}$$

Inserting (3.6.2) in (3.6.4) we find

$$G(|v_r|) = -\frac{1 - p}{e^{a/\tau|v_r|} - pe^{-a/\tau|v_r|}} \tag{3.6.5}$$

Therefore, the deviated distribution function for a cylinder is

$$\widetilde{N} = R\tau\left[1 - \frac{1 - p}{e^{a/\tau|v_r|} - pe^{-a/\tau|v_r|}}e^{-r/\tau v_r}\right] \tag{3.6.6}$$

Note that in the limit $a \longrightarrow \infty$ we retrieve the bulk value for the deviation given by $R\tau$.

Chapter 4

Theory of lattice thermal conductivity

Application of a temperature gradient in solids excites elementary excitations such as free electrons and phonons, which conduct heat from the hotter to the colder end of the material. In dielectrics and semi conductors almost all heat is conducted by phonons. Heat conduction in solids is described by the lattice thermal conductivity of the material. In this chapter we present the theory of the lattice thermal conductivity based on the Boltzmann transport equation and the relaxation time approximation. Moreover, we provide an expression for the thermal conductivity of a cylindrical wire.

4.1 Thermal conductivity

When a finite temperature gradient is applied across a solid, we find that in the steady state the rate of heat energy flow per unit area is given by the Fourier law

$$Q = -\kappa \nabla T \tag{4.1.1}$$

where κ is the thermal conductivity. The heat current Q can be found by summing over contributions from all phonon modes as in (3.2.6)

$$\begin{aligned} Q &= \frac{1}{V} \sum_{\mathbf{k}s} \hbar\omega(\mathbf{k}s) N_{\mathbf{k}s} v_s(\mathbf{k}) \\ &= \frac{1}{V} \sum_{\mathbf{k}s} \hbar\omega(\mathbf{k}s) \widetilde{N}_{\mathbf{k}s} v_s(\mathbf{k}) \end{aligned} \tag{4.1.2}$$

where V is the volume of the solid, and the second equality in (4.1.2) is a result of noting that only the deviation from the equilibrium distribution function contributes to the thermal current.

Combining (4.1.1) and (4.1.2) we find an expression for the thermal conductivity

$$\kappa = -\frac{1}{V|\nabla T|^2}\sum_{\mathbf{k}s}\hbar\omega(\mathbf{k}s)\widetilde{N}_{\mathbf{k}s}\mathbf{v}_{\mathbf{s}}.\nabla T \tag{4.1.3}$$

Thus by using the appropriate expression for the deviated distribution function $\widetilde{N}_{\mathbf{k}s}$ the thermal conductivity can be evaluated for different geometries.

4.2 Scattering rates

In the harmonic approximation discussed in section 2.1 the lattice waves are decomposed into normal modes which do not interact with each other. In this approximation there will be no resistance to heat flow and therefore the thermal conductivity will be infinite. However, real crystals do in fact have a finite thermal conductivity as a result of phonon scattering. In dielectrics phonons primarily scatter with themselves. Crystals may also contain defects and impurities which result in phonon-impurity scattering. In addition, the finite size of small crystals inevitably leads to boundary scattering. These phonon scattering mechanisms result in a thermal resistance, and ultimately a finite thermal conductivity. Thus the study of phonon scattering mechanisms is crucial in the theory of lattice thermal conductivity.

If we consider the third order term of the potential (2.1.1) as a perturbation to the original Hamiltonian i.e $H^{'} \sim x^3$, and by using Fermi's golden rule we find that this term acts as a mechanism for two phonons to merge into a third or for one to split into two. Such processes are called three-phonon processes and are often referred to as anharmonic processes as they result from the deviation of the crystal Hamiltonian from the Harmonic approximation. Higher order terms in the crystal Hamiltonian result in four phonon processes, but since the anharmonicity of the Hamiltonian rises at higher temperatures, at relatively low temperatures it is sufficient to consider the expansion of the crystal potential up to third order only.

For three-phonon processes energy conservation gives

$$h\nu + h\nu^{'} = h\nu^{''} \tag{4.2.1}$$

where two phonons of frequency ν and $\nu^{'}$ merge to form a phonon of frequency $\nu^{''}$, or the phonon with frequency $\nu^{''}$ splits into the other two phonons.

Momentum conservation on the other hand takes the following form

$$\mathbf{k} + \mathbf{k}^{'} - \mathbf{k}^{''} = \mathbf{G} \tag{4.2.2}$$

where $\mathbf{G}$ is a reciprocal lattice vector and $\mathbf{k}$, $\mathbf{k}^{'}$, and $\mathbf{k}^{''}$ are the wave vectors of the three phonons. If $(\mathbf{k}+\mathbf{k}^{'})$ falls within the first Brillouin zone then $\mathbf{G}=0$, otherwise $\mathbf{G}\neq 0$. This is due to the fact that the allowable wave vector for a lattice vibration is confined to the first Brillouin zone. For $\mathbf{G}=0$ the phonon scattering process is called a Normal process (N-processes) and for $\mathbf{G}\neq 0$ it is called an Umklapp process (U-processes). If the U-processes are not considered the thermal conductivity of an infinite crystal would still be infinite because N-processes conserve both the energy and momentum, thus causing no resistance. In U-processes on the other hand, the reciprocal lattice vector present changes the net direction of phonon propagation which creates a thermal resistance to the heat flow.

Approximate expressions for the scattering relaxation times in terms of frequency have been found by [16]. For the three phonon U-processes a commonly used expression is [3]

$$\tau_U^{-1} = B_U T^3 \omega^2 \tag{4.2.3}$$

where

$$B_U = \frac{\hbar\gamma^2}{Mv^2\theta_D} e^{-\theta_D/cT} \tag{4.2.4}$$

Here θ_D is the Debye temperature, v is the group velocity, M is the average mass of an atom in the solid, and γ is the *Grüneisen* parameter, and c is a constant relating to the material.

The *Grüneisen* parameter can be obtained from the heat capacity at constant volume $C(\mathbf{k}s)$ and the single mode *Grüneisen* parameter $\gamma_{\mathbf{k}s} = -\dfrac{V}{\omega(\mathbf{k}s)}\dfrac{\partial\omega(\mathbf{k}s)}{\partial V}$ using the definition

$$\gamma = \frac{\sum\limits_{\mathbf{k}s} \gamma_{\mathbf{k}s} \times C(\mathbf{k}s)}{\sum\limits_{\mathbf{k}s} C(\mathbf{k}s)} \tag{4.2.5}$$

For N-processes a similar expression is used [3]

$$\tau_N^{-1} = B_N \omega^f T^g \tag{4.2.6}$$

with

$$B_N = \left(\frac{k_B}{\hbar}\right)^f \frac{\hbar\gamma^2 V_a^{(f+g-2)/3}}{Mv^{f+g}} \tag{4.2.7}$$

in which V_a is the volume per atom, and the constants (f, g) may take the values $(1, 3)$ or $(1, 4)$.

The relaxation time due to impurity and defect scattering is highly frequency dependent and is usually written as (cf. A.1)

$$\tau_I^{-1} = A\omega^4 \tag{4.2.8}$$

where A is a temperature independent constant.

Boundary scattering is also usually included by making use of the so called Casimir limit [25] which gives the boundary scattering relaxation time in the following form

$$\tau_B^{-1} = F\frac{v}{L} \tag{4.2.9}$$

where v is the phonon group velocity, L is a characteristic length of the material, and F is a fitting parameter.

The total relaxation time is thus obtained by combining these expressions as in (3.3.12). We also mention that in addition to the boundary scattering relaxation time we include the effect of the boundary in finite structures within the expression of the distribution function as we saw in the previous chapter.

4.3 Thermal conductivity in bulk materials

As we have seen in section 4.1 the evaluation of the lattice thermal conductivity requires the knowledge of the deviated phonon distribution function $\widetilde{N}$.

Using expression (3.4.3) for the deviated distribution function in (4.1.3) and converting the summation over the wavevectors into integration we obtain the thermal conductivity of bulk materials

$$\kappa_{bulk} = \frac{1}{(2\pi)^3}\sum_s \int 4\pi k_s^2 \left[\int \tau v_s^2 \frac{\hbar^2\omega_s^2}{k_B T^2}\frac{e^{\hbar\omega_s/k_BT}}{(e^{\hbar\omega_s/k_BT}-1)^2}\cos^2\theta\frac{d\Omega}{4\pi}\right]dk_s \tag{4.3.1}$$

where θ is the angle between the thermal gradient and the phonon group velocity, and $d\Omega = \sin\theta d\theta d\phi$ is the solid angle in the direction of the group velocity.
Thus, we have

$$\kappa_{bulk} = \frac{1}{(2\pi)^3}\sum_s \int 4\pi k_s^2 \left[\int_0^{2\pi} d\phi \int_0^{\pi} \tau v_s^2 \frac{\hbar^2\omega_s^2}{k_B T^2}\frac{e^{\hbar\omega_s/k_BT}}{(e^{\hbar\omega_s/k_BT}-1)^2}\cos^2\theta \frac{\sin\theta d\theta}{4\pi}\right] dk_s$$
$$= \frac{1}{3}\sum_s \frac{1}{2\pi^2 v_s^3}\int_0^{\omega_D}\left[\tau v_s^2 \frac{\hbar^2\omega_s^2}{k_B T^2}\frac{e^{\hbar\omega_s/k_BT}}{(e^{\hbar\omega_s/k_BT}-1)^2}\right]\omega_s^2 d\omega_s \tag{4.3.2}$$

where ω_D is the Debye frequency, and a linear dispersion relation was used.

Hence,

$$\kappa_{bulk} = \frac{1}{3}\sum_s \int \tau v_s^2 C(\omega_s) d\omega_s \tag{4.3.3}$$

where

$$C(\omega_s) = \hbar\omega_s D(\omega_s)\frac{d\overline{N}}{dT} \tag{4.3.4}$$

is the phonon specific heat, and $D(\omega)$ is the density of states.

If τ is frequency independent then we arrive at the kinetic theory expression of thermal conductivity

$$\kappa = \frac{1}{3} C v \Lambda \tag{4.3.5}$$

where $\Lambda = \tau v$ is the phonon mean free path.

Defining $x = \hbar\omega/k_BT$, then (4.3.2) then takes the form

$$\kappa_{Bulk} = \frac{1}{3}\sum_s \frac{k_B}{2\pi^2 v_s}\left(\frac{k_B T}{\hbar}\right)^3 \int_0^{\theta_D/T} \tau(x)\frac{x^4 e^x}{(e^x-1)^2} dx \tag{4.3.6}$$

The total relaxation time in (4.3.6) includes the phonon-phonon, phonon-impurity, and phonon boundary scattering.

At low temperatures the thermal conductivity is dominated by boundary scattering and follows the T^3 dependence of the specific heat. As temperatures increase boundary scattering becomes less important and the thermal conductivity increases until it reaches a maximum at intermediate temperatures, after which it starts to decrease. The decrease is brought upon by the enhanced impurity and phonon-phonon scattering. As temperatures increase further phonon-phonon scattering becomes predominant, and the thermal conductivity is further reduced and tends to a constant value at very high temperatures.

4.4 Expression for the thermal conductivity of a cylindrical wire

The thermal conductivity of cylindrical wires may be evaluated by using expression (3.6.6), which we derived for the cylindrical geometry, in (4.1.3) and averaging over the wire cross-section. Since the area of an annulus is proportional to rdr then the thermal conductivity of the wire is given by

$$\kappa(T) = \frac{2k_B}{Va^2}\sum_{\mathbf{k}s}\left\{\left(\frac{\hbar\omega_s(\mathbf{k})}{k_BT}\right)^2 \frac{e^{\hbar\omega_s(\mathbf{k})/k_BT}}{(e^{\hbar\omega_s(\mathbf{k})/k_BT}-1)^2}\tau v^2(\mathbf{k}s)\times \int_0^a\left[\left(1+G(|v|)e^{-r/\tau v}\right)\right]rdr\right\} \tag{4.4.1}$$

Carrying out the integration in r and plugging in the value of G we get

$$\kappa(T) = \frac{k_B}{V}\sum_{\mathbf{k}s}\left\{\left(\frac{\hbar\omega_s(\mathbf{k})}{k_BT}\right)^2 \frac{e^{\hbar\omega_s(\mathbf{k})/k_BT}}{(e^{\hbar\omega_s(\mathbf{k})/k_BT}-1)^2}\tau v^2(\mathbf{k}s)\times \left[1-\frac{2(1-p)}{\xi^2\Big(e^{\xi}-pe^{-\xi}\Big)}\Big(1-\big(1+\xi\big)e^{-\xi}\Big)\right]\right\} \tag{4.4.2}$$

in which $\xi = a/\Lambda$ is the non-dimensional wire thickness and Λ is the phonon mean free path.

We note that the first term in the square brackets of (4.4.2) gives the bulk thermal conductivity, while the second is due to the size effects in the wire. The minus sign means that the thermal conductivity of the wire will be diminished with respect to its bulk value. In the case of total specular reflection i.e $p = 1$ we retrieve the bulk expression for the thermal conductivity as expected, since in this case the phonons change direction only in the r-direction. As a result the flux in the z-direction remains unchanged. However, the phonon group velocities in the NW are lower than that of their bulk counterparts and therefore, the conductance of a completely polished surface NW will still be lower than that of the bulk.

The magnitude of the wavevector in (4.4.2) is given by (2.10.6) and the summation can be changed into a summation over the wavevector components k_r while an integration over k_z is employed, since the wire may be considered infinite in the z-direction so that the number of modes is large

$$\kappa(T) = \frac{k_B}{V}\sum_j\sum_{k_r}\int_{-\pi/d}^{\pi/d} f_j(\xi)\left\{\left(\frac{\hbar\omega_j}{k_BT}\right)^2 \frac{e^{\hbar\omega_j/k_BT}}{(e^{\hbar\omega_j/k_BT}-1)^2}\Lambda_j\overline{v}_j\frac{dk_z}{\frac{(2\pi)}{L}}\right\} \tag{4.4.3}$$

Here d is the interatomic spacing so that the integration is taken over the entire Brillouin zone, L is the length of the wire, $\overline{v}_j$ is the averaged phonon group velocity of the jth branch, and

$$f_j(\xi) = \left[1 - \frac{2(1-p)}{\xi^2\left(e^{\xi} - pe^{-\xi}\right)}\left(1 - \left(1+\xi\right)e^{-\xi}\right)\right] \tag{4.4.4}$$

The allowed discretized values of the wavevector components k_r are determined by either (2.10.14) for the clamped boundary condition or (2.10.17) for the free surface boundary condition.

The number of points in k-space may be estimated by the number of atoms along the radial and azimuthal directions.

The atoms in the Azimuthal direction are considered to lie on a chain lattice of length $2\pi a$ separated by the mean interatomic spacing d, so that the Azimuthal number n may run from 0 up to $2\pi a/d$. Similarly the atoms vibrating in the radial direction can be visualized as being located on a linear chain of length $2a$, thus the number of zeros for each value of n is estimated to be $2a/d$.

The integrand in (4.4.3) is an even function of k_z so that the integration can be taken as twice that from 0 to π/d, and using $kdk = k_z dk_z$ we find

$$\kappa(T) = \frac{k_B}{\pi^2 a^2}\sum_j\sum_{k_r}\int_0^{\pi/d} f_j(\xi)\left(\frac{\hbar\omega_j}{k_BT}\right)^2 \times \frac{e^{\hbar\omega_j/k_BT}}{(e^{\hbar\omega_j/k_BT}-1)^2}\Lambda_j\overline{v}_j\frac{kdk}{\sqrt{k^2-k_r^2}} \tag{4.4.5}$$

Let $x = \hbar k\overline{c}_j/k_BT$, where $\overline{c}_j$ is an averaged phase velocity, then

$$\kappa(T) = \frac{k_B}{\pi^2 a^2}\sum_j\sum_{k_r}\left(\frac{k_BT}{\hbar\overline{c}_j}\right)\int_{x_{min}}^{x_{max}} f_j(\xi)\times \frac{x^3e^x}{(e^x-1)^2}\Lambda_j\overline{v}_j\frac{dx}{\sqrt{x^2 - \left(\frac{\hbar\overline{c}_j}{k_BT}\right)^2 k_r^2}} \tag{4.4.6}$$

and the limits of integration are given by

$$x_{min} = \frac{\hbar \overline{c}_j}{k_B T} k_r, \quad x_{max} = \frac{\hbar \overline{c}_j}{k_B T} \sqrt{(\pi/d)^2 + k_r^2} \tag{4.4.7}$$

In order to evaluate (4.4.6) we must provide an expression for the total relaxation time τ (or equivalently the mean free path Λ). This can be done by combining the mass difference scattering relaxation time (A.1.22) and the U-processes relaxation time (4.2.3) along with a boundary scattering relaxation rate given by $(1-p)\overline{v}_j/2(1+p)a$ using the Matthessien rule:

$$\begin{aligned} \tau^{-1} &= \tau_{md}^{-1} + \tau_U^{-1} + \tau_B^{-1} \\ &= Ex^4 + Dx^2 + \frac{(1-p)\overline{v}_j}{2(1+p)a} \end{aligned} \tag{4.4.8}$$

where,

$$E = \frac{\Gamma_{md} V_u}{4\pi \overline{v}_j^3} \left(\frac{k_B T}{\hbar} \right)^4, \quad \text{and} \quad D = B_U T^2 \left(\frac{k_B T}{\hbar} \right)^2 \tag{4.4.9}$$

Chapter 5

Results and discussion

In this chapter we present calculations of thermal conductivity of Silicon (Si) NWs based on the model discussed in the previous chapters. The results are analyzed and compared to experimental measurements of thermal conductivity of bulk and individual Si NWs found in the literature.

5.1 Thermal conductivity of clamped surface Si nanowires

The thermal conductivity of a cylindrical NW can now be obtained by numerically evaluating the integral in (4.4.6) for each phonon branch and summing over the contributions of all the branches. It is found that the contribution to the thermal conductivity decreases as we go higher in the dispersion branches due to the flattening of their slopes, as can be seen in the dispersion curves of a cylindrical solid presented in chapter 2. Hence, the summation over the phonon branches in (4.4.6) converges and the main contribution comes from the first few lowest frequency branches in each case. In addition, it is found that the main contribution to the thermal conductivity is from the longitudinal and torsional vibration modes as shown in Figure 5.1.

In numerical calculations the averaged interatomic spacing d in Silicon is taken to be 5.431 Å and an averaged value of 355.3 K is given for the Debye temperature based on experimental measurements reported by [3]. In addiction, the Grüneisen parameter is not considered to deviate from its bulk value since it is a material property and a mean value of 0.77 is used [3]. Normal phonon processes are not included in the calculations since they do not create direct resistance to the thermal current and are dominated by boundary scattering. The averaged phonon velocities are found from the dispersion curves of an elastic cylinder found in chapter 2. As we have seen from Figure 2.5 the group velocity of confined phonons is much lower than that of the bulk. Consequently, the thermal

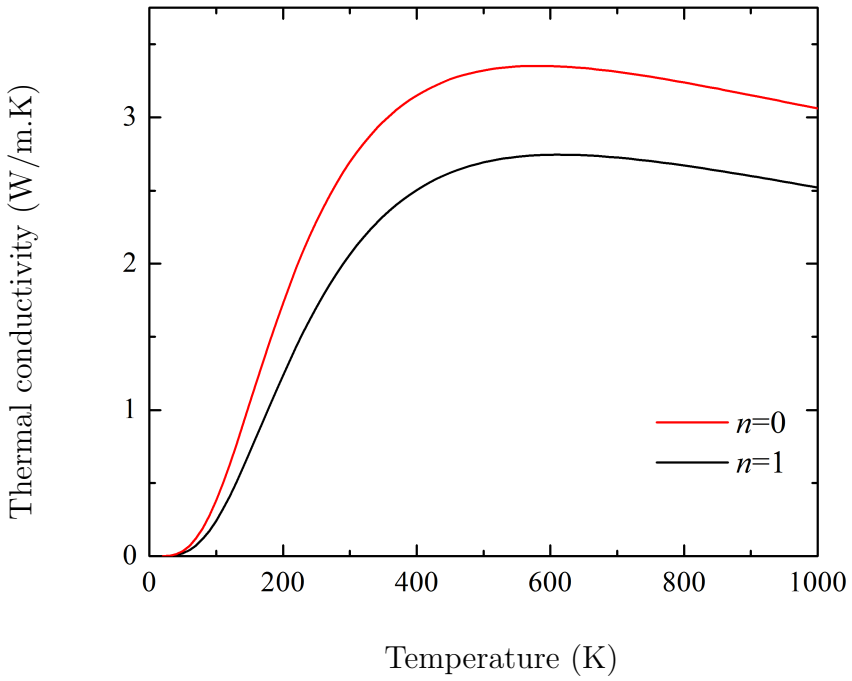

Figure 5.1: Contributions of the longitudinal and torsional ($n = 0$) modes to the thermal conductivity along with that of the flexural modes ($n = 1$) in a 5 nm radius clamped NW with $p = 0.5$.

conductivity of the NWs is expected to be substantially reduced in comparison to the bulk.

The specularity parameter is considered to be a constant which can take values from 0 to 1. In Figure 5.2 the thermal conductivity curves of clamped surface NWs for an intermediate value of 0.5 are presented. The size effect is apparent form the figure and as expected the thermal conductivity of the NWs is significantly low and decreases with decreasing wire radius. The decrease in the thermal conductivity from the 11 nm NW to the 5 nm NW can be attributed to the decrease in the number of vibration modes as the wire cross-section decreases.

The trend followed by the curves is as follows: at low temperatures starting from 15 K the conductivity is very low due to low phonon group velocities and enhanced boundary and confinement effects, as the temperature increases the thermal conductivity increases and reaches a maximum of about 14 W/m.K at around 540 K for the clamped 11 nm radius NW, while it reaches a maximum of about 6 W/m.K at around 700 K for the 5 nm radius NW. This is in sharp

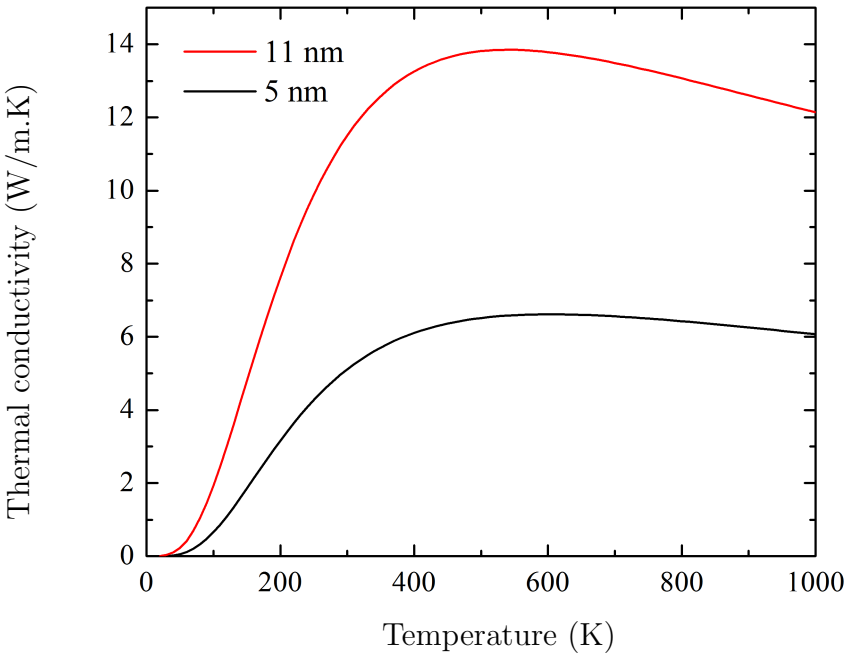

Figure 5.2: Thermal conductivity curves for clamped surface Si NWs of radii 5 and 11 nm given by (4.4.6) with $p = 0.5$.

contrast to the peak of bulk Si that occurs at about 25 K. The peaks seem to shift to higher temperatures as the wire diameter is decreased. This suggests that the increase of phonon boundary scattering dominates over the phonon-phonon umklapp scattering up to higher and higher temperatures as the wire diameter is decreased. As the temperature increases further phonon-phonon and impurity scattering become more efficient thus causing the decrease at high temperatures.

It is interesting to show the behavior of the thermal conductivity in bulk silicon as compared to that in a clamped silicon NW. This is illustrated in Figure 5.3 where measurements on thermal conductivity of bulk silicon reported in [3] are compared to the results obtained from the present calculation for a clamped Si NW of diameter 22 nm based on (4.4.6) with specularity $p = 0.2$. It is seen from Figure 5.3 that the thermal conductivity of bulk Si is much higher than that of the NW over the entire temperature range indicated. In addition, the large shift between the peaks of each curve is also clear from the figure. The results illustrated in Figures 5.2 and 5.3 show a strong dependence of the thermal conductivity on the NW diameter or cross-section. This is ascribed to the size effects that arise in nanostructures which leads to increased phonon-boundary scatter-

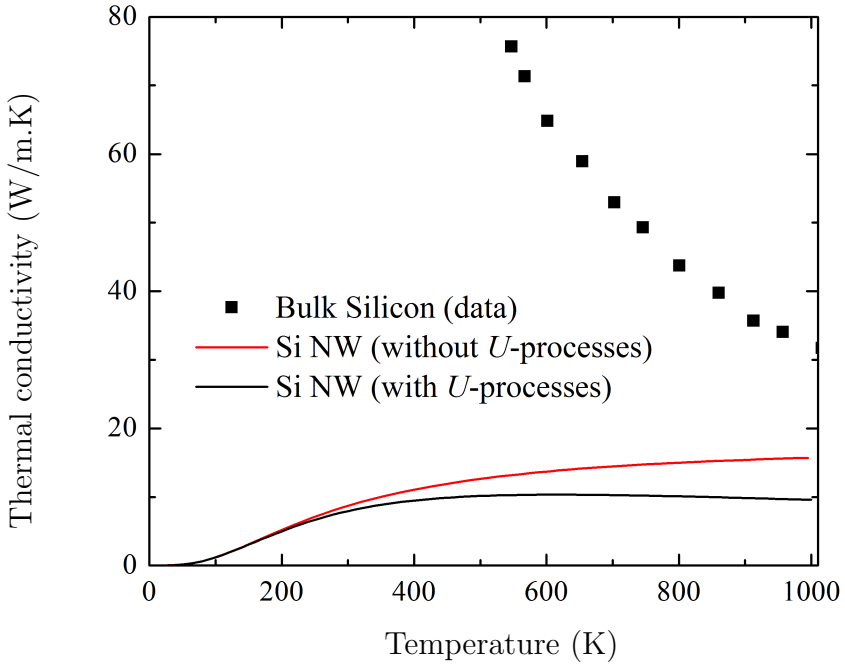

Figure 5.3: Thermal conductivity of a clamped 22 nm diameter Si NW based on the present model calculations (with p=0.2) with and without U-processes, compared with the thermal conductivity of bulk Si from experimental data reported by Morelli *et al* [3].

ing. The decrease in the thermal conductivity in the NW as compared to the bulk might also be a result of phonon spectrum modification which was modeled by using confined phonon velocities and a spatially dpendent phonon distribution function, as detailed in sections 2.8, 2.10, and 3.6. At high temperatures the NW thermal conductivity is expected to increase closer to that of the bulk due to the reduction of phonon-boundary scattering, in addition to the increase of the confined phonon group velocities in this temperature regime (cf. Figure 2.5). Nevertheless, the thermal conductivity of the NW is still much lower than that of the bulk at high temperatures. This is due to the anharmonic phonon-phonon processes which lead to a reduction of the phonon mean free path at high temperatures (see the surve with U-processes in Figure 5.3). It is however emphasized that the thermal conductivity of the NW remains lower than that of the bulk even at very high temperatures simply because of the lower group velocities in the NW.

The effect of surface is investigated with the help of the specularity parameter p introduced in section 3.6. Figure 5.4 shows several results which are summarized

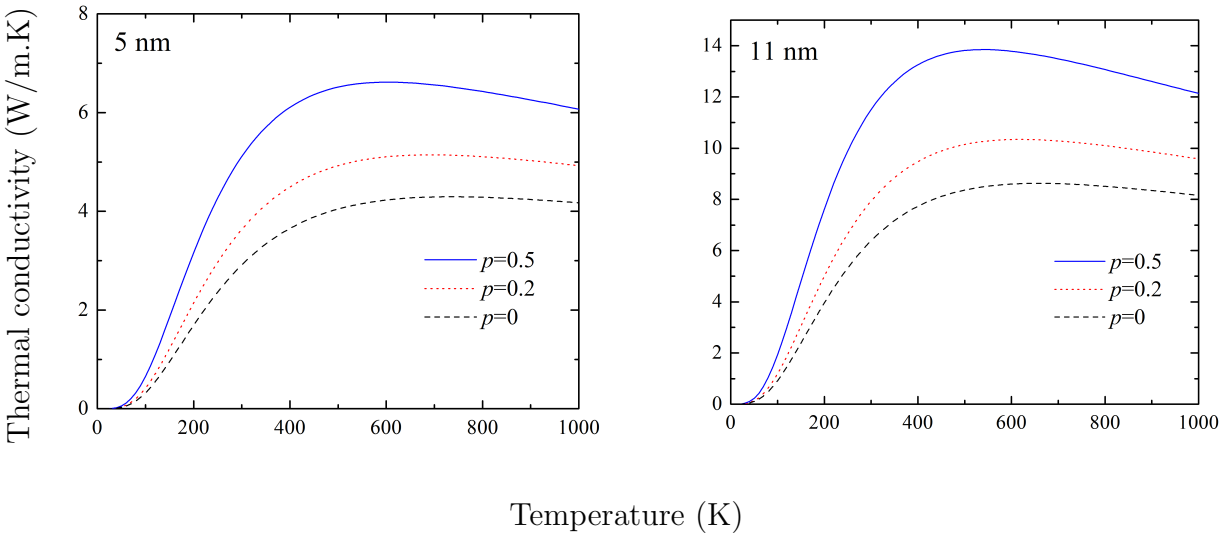

Figure 5.4: Variation of the thermal conductivity of clamped surface NWs of radii 5 and 11 nm with respect to the specularity parameter p.

as follows: (i) As the surface roughness increases (i.e p decreases), the thermal conductivity decreases, since a larger fraction of phonons undergoes diffuse scattering at the wire surface, resulting in slow thermal transport. This is in contrast to the case of a polished surface, where the incident phonons are simply reflected creating no resistance to the thermal current, and thus enabling a higher thermal conductivity. The effect of phonon diffuse scattering on the thermal conductivity is apparent from (4.4.2) since as the specularity parameter tends to zero the second term in the square brackets becomes a large negative value resulting in a decrease in $\kappa(T)$. (ii) The figure also shows that the peaks of the thermal conductivity shift to lower temperatures with increasing p due to the decrease in phonon-boundary scattering. For example, for a NW with radius 11 nm (Figure 5.4 right panel), the peaks occur at 650 K ($p = 0$), 620 K ($p = 0.2$), and 540 K ($p = 0.5$). Similarly, the same shifting is observed in the left panel of Figure 5.4. Therefore, we may conclude that as the surface roughness is reduced the peaks in the thermal conductivity shift to lower temperatures closer to that of the bulk.

5.2 Comparison with experimental measurements

Measurements on thermal conductivity of individual Si NWs have been reported by Li *et al* [4]. The Si NWs were synthesized by the vapor-liquid-solid method, in which Au clusters were used as a solvent at high temperature. The Si and Au formed a liquid alloy and when the alloy became supersaturated with Si, Si

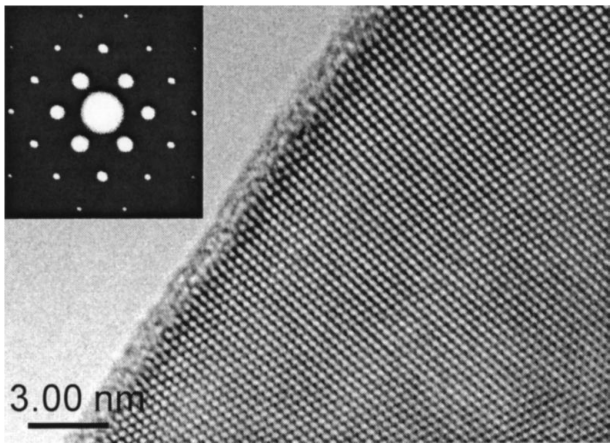

Figure 5.5: High-resolution TEM image of a 22 nm single crystal Si NW. The inset is a selected area electron diffraction pattern of the NW. Reproduced from [4].

NWs grew by precipitation at the liquid-solid interface. Using a high-resolution transmission electron microscopy (TEM) investigation the authors were able to determine that the Si NWs were single crystalline (see Figure 5.5) and grew along the (111) direction. The wire diameters fell in the range of 10-200 nm and the lengths were several microns.

The synthesized NWs were then drop cast onto suspended heater devices so that individual Si NWs thermally connected the two devices. The heater devices consisted of two suspended microfabricated microstructures. The suspended microstructures consisted of two silicon nitride (SiN_x) membranes. A thin Pt resistance coil and a separate Pt electrode were patterned onto each membrane, each serving as a heater to increase the temperature of the suspended island, as well as a resistance thermometer to measure the temperature of each island.

By applying a bias voltage to one of the resistors the authors were able to increase the temperature of one of the heaters above the thermal bath temperature through Joule heating. Under steady state, part of the heat flowed through the NWs to the other resistor, raising its temperature. By solving the heat transfer equations of the system, the authors were able to relate the temperatures of the resistors to the conductance of the wires and the suspending legs along with the electrical power of the heating resistor and the total electrical lead resistance of Pt lines that connects the heater coil. The thermal conductivity of the bridging NW was then estimated from the slope of the measured temperature versus power after considering the diameter and length of the wires. All the measurements were carried out at a high vacuum level of 2×10^{-6} Torr and temperature ranging up to 320 K.

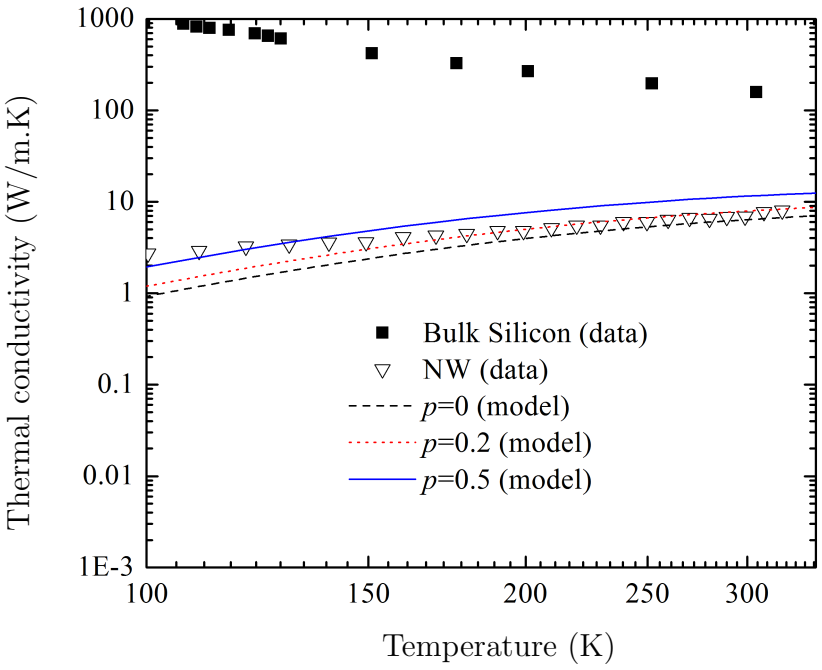

Figure 5.6: Comparison of the thermal conductivity of a clamped 22 nm diameter Si NW based on the present model with experimental data on a Si NW of the same diameter [4] along with bulk Silicon [3].

The authors presented thermal conductivity measurements for NWs of diameters 22, 37, 56, and 115 nm. The thermal conductivity was found to be more than two orders of magnitude lower than the bulk value. In addition, the conductance was shown to decrease with decreasing wire diameter. The authors attributed this strong diameter dependence of the thermal conductivity in the NWs to increased phonon-boundary scattering with decreasing wire diameter.

The results of the measurements clearly indicate that enhanced boundary scattering has a strong effect on phonon transport in Si NWs which justifies the reasoning behind the details of our model.

As can be seen from Figure 5.5 the synthesized Si NWs are enclosed by a thin oxide layer which serves to clamp the wire. Therefore, these measurements may be compared to the results of our model on clamped Si NWs. Such a comparison between the model results on clamped 22 nm diameter Si NWs with experimental measurements is shown in Figure 5.6. The agreement with the experimental data is evident from the figure. It can be seen that at low temperatures the measured

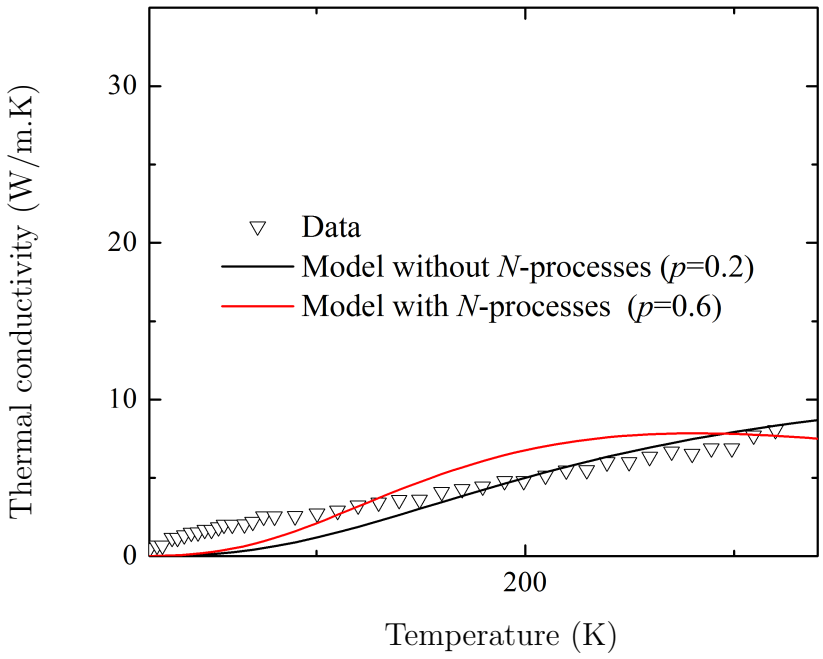

Figure 5.7: Comparison of thermal conductivity curves with and without N-processes obtained from the present model for a clamped 22 nm diameter Si NW, along with experimental measurements reported in [4].

thermal conductivity follows the trend of the $p = 0.5$ curve, while it follows the trend of the $p = 0$ curve at high temperatures and the $p = 0.2$ curve at intermediate temperatures. This is of course expected, since the surface roughness depends on the phonon wavelength, which in turn is temperature dependent. For long wavelengths the surface will look perfectly smooth, whereas for shorter wavelengths the same surface will appear rough. Thus at low temperatures the surface will appear to be perfectly polished, as a result the experimental curve agrees with the $p = 0.5$ curve in this range. At higher temperatures the phonon wavelengths become shorter which results in the agreement of the experimental curve with the $p = 0$ curve.

It is worth noting that the measured thermal conductivity of the 22 nm diameter NW did not exhibit a peak within the experimental temperature range. On the other hand, the authors found that for the 37, 56, and 115 nm diameter wires, thermal conductivities reached peak values at around 210, 160, and 130 K, respectively. The model calculations have shown that the thermal conductivity of the 22 nm diameter NW peaks in the temperature range 540-650 K and

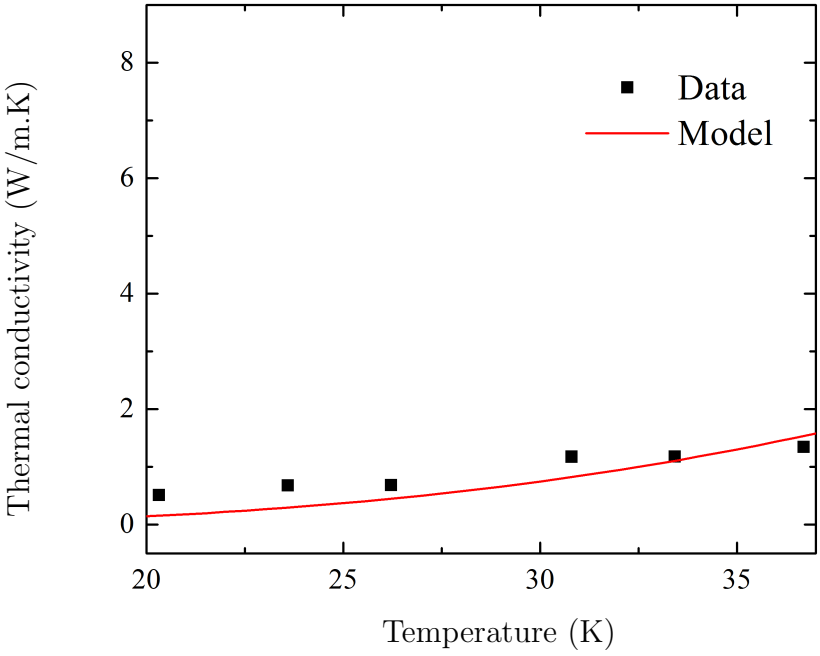

Figure 5.8: Comparison between model results on an 11 nm radii clamped NW with $p = 0.98$ and the experimental data at low temperatures.

that of the 10 nm nanowire at around 700 with the U-processes included (cf. section 5.1). Thus the model results are in agreement with the experimentally observed behavior. On the other hand, excluding the U-processes in the model calculations resulted in no peak in the thermal conductivity even up to 1000 K. As there was no peak observed in the experimental measurements on the 22 nm diameter NW, it might be that for NWs with diameters equal to or smaller than 22 nm the thermal transport becomes ballistic. That is, the phonons no longer exhibit phonon-phonon scattering and travel in almost straight lines until they are scattered by the boundary. However, the lack of experimental data at high temperatures means that the exact behavior cannot be accurately predicted. As discussed in section 5.1 the shift of the peak to higher temperatures is due to phonon boundary scattering dominating phonon-phonon scattering in the NW. This suggests that phonon-phonon scattering, and especially normal phonon-phonon scattering, does not play an important role in governing thermal transport in the wires, and thus N-processes may be neglected. To illustrate this point, calculations were carried out with N-processes included using the relaxation time (4.2.6) with $(f, g) = (1, 3)$. The results are shown in Figure 5.7. It can be seen from the figure that with the N-processes included the conductivity

peaks at a much lower temperature near 280 K. In addition, the trend of the measured thermal conductivity agrees better with the curve that excludes the normal processes. It is also apparent from the figure that the model results lead to an overestimation of phonon boundary scattering at very low temperatures since the model curves are much lower than that of the measurements in this temperature range. However, this discrepancy between the model calculations and the experimental measurements may be attributed to experimental errors. It should be noted that the measured thermal conductivity includes the thermal conductance of the junction between the NW and the suspended islands in addition to the intrinsic thermal conductance of the NW itself. Thus the measured thermal conductivity at low temperatures may be much lower than reported. However, the authors estimated the thermal conductance of the junctions with the carbon deposition, and found that the junction contribution is less than 15% of the total thermal transport barrier. Another source of measurement error might be due to heat transfer between the two membranes via radiation and air conduction, in addition to a 0.3 nm uncertainty in the measurement of the NW diameters, which were measured using a tapping mode atomic force microscope [35]. Nevertheless, as can be seen from Figure 5.8, a better agreement with the experimental measurements at low temperatures may be obtained by noting that at very low temperatures the surface appears to be perfectly smooth so that a specularity parameter closer to 1 must be used. A better fit with the experimental data over the entire temperature range may be obtained by using the wavelength dependent expression (3.6.3) for the specularity parameter. However, in this case uncertainty will arise regarding the mean surface roughness since the actual value cannot be accurately measured and thus will have to be estimated or fitted to the experimental data. This in turn, will only serve to complicate the computation without providing any further information.

5.3 Thermal conductivity of free surface NWs and thermal current modulation

Making use of the dispersion relations of a free surface cylinder found in section 2.9 along with the velocity averaging method detailed in section 2.8 and summing over the wavevector components given by (2.10.17), we may obtain the thermal conductivity of a free surface NW by means of (4.4.6). The thermal conductivity of a free surface NW exhibits the same characteristics as that of clamped cylindrical NWs with regards to curve trend. The curve peaks also seemed to shift to lower temperatures as the specularity parameter was increased, as can be seen from Figure 5.9, just like the clamped surface NWs (cf. section 5.1). The peaks also shift to higher temperatures as the wire cross-section is decreased.

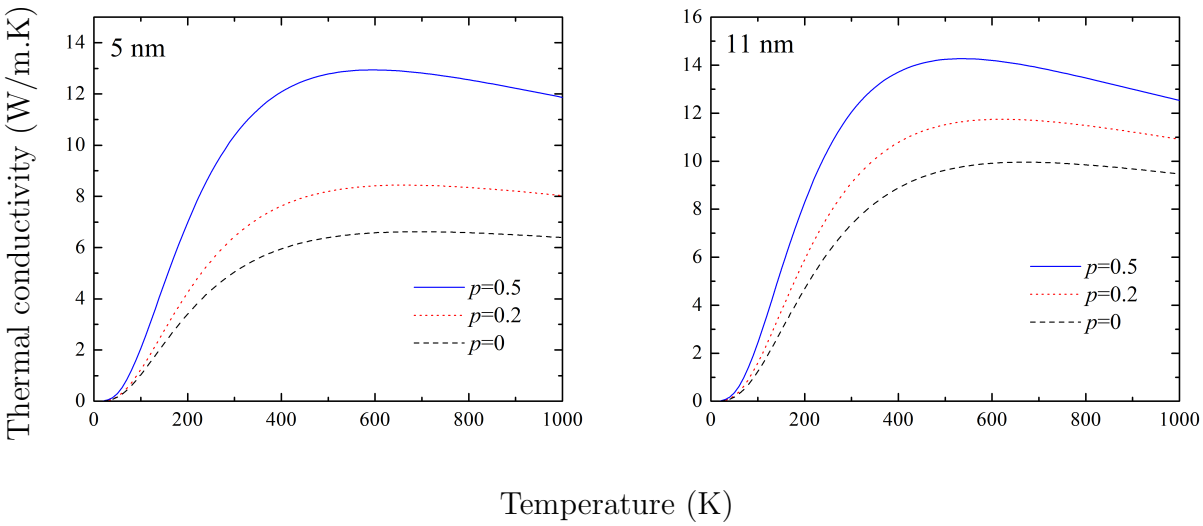

Figure 5.9: Variation of the thermal conductivity of free surface NWs of radii 5 and 11 nm with respect to the specularity parameter p.

An outstanding difference between the free surface and clamped NWs is that the thermal conductivity of a free surface NW was observed to be larger than that of a clamped NW. This effect seems to be enhanced as the NW cross-section is reduced which is evident in Figure 5.10. The thermal conductivity of the free surface 11 nm radius NW is slightly higher than that of the clamped NW. On the other hand, for the 5 nm radius NW the thermal conductivity for the free surface boundary condition is significantly larger than that of the camped boundary condition and almost doubles that of a clamped NW at 300 K, representing a 100% increase.

The difference between the thermal conductivities of the clamped and free surface NWs may be ascribed to phonon spectrum modification due to the changing surface conditions. It is found that the number of dispersion branches increases for the free surface boundary condition. In addition, the branches of the free surface NW shift to lower frequencies, thus giving a greater contribution to the thermal conductivity. It can also be seen from the wavevector components (2.10.14) and (2.10.17) that the phonon frequencies in the case of the free surface boundary condition (Neumann) are lower than that of the clamped boundary condition (Dirichlet), since with the exception of the case were the order of the Bessel functions is 0 the zeros of the derivative of the Bessel functions are smaller than that of the Bessel functions themselves. The fact that the phonon frequencies are higher for the clamped boundary conditions results in the observed lowering in the thermal conductivity. This can be seen from the expression of the thermal con-

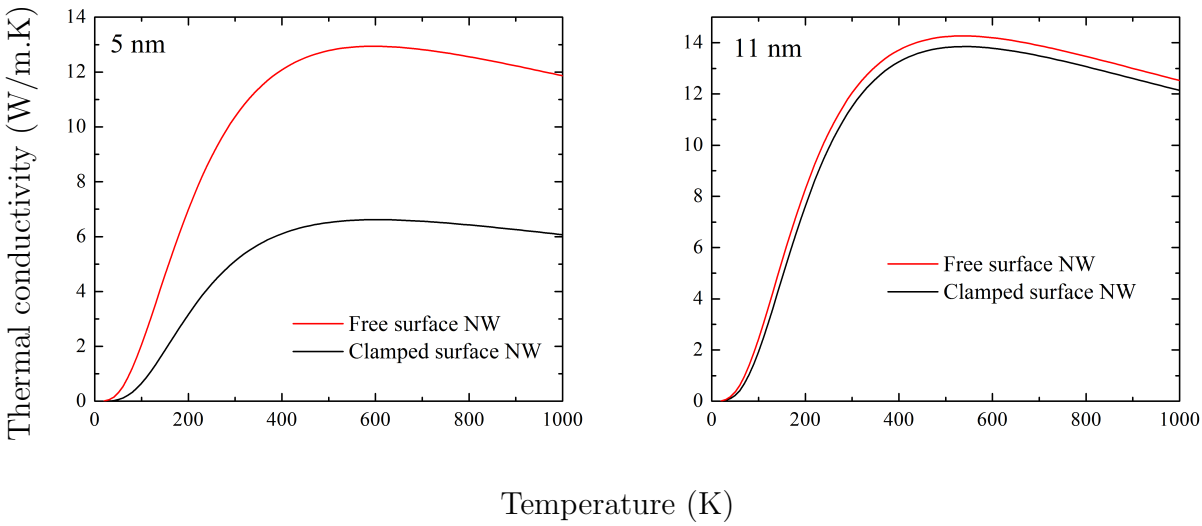

Figure 5.10: Comparison between the thermal conductivity of clamped and free surface NWs of radii 5 and 11 nm.

ductivity, since the integrand in (4.4.6) is dominated by the term $x^3e^x/(e^x-1)^2$, and for low temperatures this term tends to x^3e^{-x}, thus the contribution of the high frequency branches to the thermal conductivity decays exponentially. This phenomenon is known as phonon softening, since as the phonons shift to lower energies it becomes easier to excite atomic vibrations in the material resulting in enhanced thermal conduction. On the other hand, the clamped surface boundary condition leads to phonon hardening resulting in a decrease in the thermal conductivity. A similar effect was observed for the specific heat of clamped and free surace NWs at very low temperatures [51], however, the enhancment of the thermal conductivity in a free surface NW occurs over the entire temperature range which makes it more practical for application purposes. It can also be seen from Figure 5.10 that this phenomenon is enhanced as the wire diameter is decreased, as a result of the increase in the surface to volume ratio. We remark that the variation between the thermal conductivities of clamped and free Si NWs could potentially find innovative applications. Tuning the surface properties and boundary conditions of the NWs can be used for engineering the thermal and electrical properties of such nanostructures. For instance, the NW boundary conditions may be used to modulate the thermal current flowing in the NWs. As the thermal current is proportional to the thermal conductivity, the significant difference between the thermal conductivity of a small diameter free NW and that of a clamped surface NW will cause a large difference in their thermal currents. Therefore, by successively clamping and releasing a small diameter NW it may be possible to modulate the thermal current, effectively creating an alternating heat

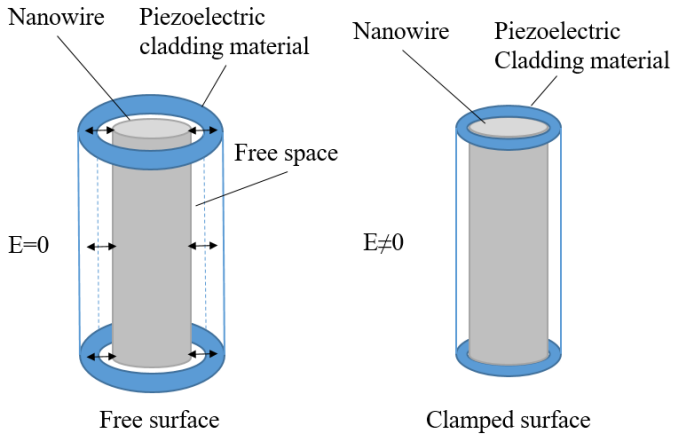

Figure 5.11: Schematic representation of a practical implementation of free and clamped nanowire boundary conditions using a Piezoelectric cladding material controlled via an external electric field.

current through the wires. The suggested method for thermal current modulation has the advantage that it is relatively simple to implement experimentally. For example, a thin Si NW may be embedded in a nanotube made of a piezoelectric material, such as quartz or aluminum nitride, so that when an external electric field is applied the piezoelectric nanotube clenches creating a clamping effect on the surface of the Si NW. An alternating external electric field thus allows for alternating between a free and clamped boundary, leading to thermal current modulation. Figure 5.11 shows a schematic representation of such a system. The modulation frequency of the external electric field can also be easily controlled, leading to a modulation of the thermal current with a controllable frequency.

Chapter 6

Conclusion

In this thesis we presented an analytical model for the calculation of lattice thermal conductivity of cylindrical nanowires (NWs). The model is based on the solution of the Boltzmann equation under the relaxation time approximation in cylindrical geometry. The objectives of our study were to interpret existing experimental measurements on thermal conductivity of Silicon (Si) NWs, and to investigate the influence of various surface effects on the thermal conductivity in NWs. Si NWs with clamped and free surface boundary conditions were considered. The dispersion relations for the clamped and free surface cylinders of diameters 10 and 22 nm were found from elasticity theory, as detailed in chapter 2. It is found that the dispersion relations consist of several branches corresponding to the various solutions of the frequency equation governing the modes of vibration of the wire. Confined phonon group velocities were obtained from the dispersion relations by employing a Boltzmann weights averaging scheme as outlined in section 2.7. It is found that the phonon group velocities are temperature dependent, and are much lower than that of the bulk. The effect of the wire borders was included in the expression of the deviated phonon distribution function. To account for elastic and inelastic phonon scattering at the wire surface a specularity parameter p was introduced in the expression of the deviated phonon distribution function (cf. section 3.6) describing the NW surface roughness. Phonon-phonon Umklapp scattering and phonon-impurity scattering along with boundary scattering were included in the relaxation time approximation using the Mattheisen rule. The radial wavevector components for free and clamped surface boundary conditions were found by solving the wave equation in cylindrical coordinates as detailed in section 2.10. The discrete radial wavevector components where summed over in the expression of the NW thermal conductivity, while integration over the axial wavevector components was employed (cf. section 4.4).

To assess the reliability of the developed model, we calculated the thermal conductivity of a clamped Si NW of 22 nm diameter and compared the results to reported experimental data on thermal conductivity of a 22 nm Si NW with

an approximately 1 nm silicon oxide layer deposited on the surface (cf. Figure 5.5) which makes the surface clamped. It is found that the results of our model are in excellent agreement with the experimental data (see Figure 5.6). At low temperatures the experimentally measured thermal conductivity agrees with the model results for specularity parameter p close to 1, while it agrees with that of specularity $p = 0$ at high temperatures, and at intermediate temperatures it agrees well with that of specularity equal to 0.2. This is attributed to the fact that the surface roughness is dependent on the phonon wavelength which varies with temperature (see section 5.2).

The calculated thermal conductivity of the NWs is found to be more than two orders of magnitude lower than that of bulk silicon. The large drop in the thermal conductivity from its bulk value is ascribed to enhanced phonon boundary scattering and phonon spectrum modification in the NWs. Moreover, the thermal conductivity of the NWs peaks at much higher temperatures than in the bulk suggesting that phonon boundary scattering dominates other scattering mechanisms to much higher temperatures in nanostructures. To illustrate this point phonon-phonon processes were enhanced by adding normal phonon-phonon processes. As expected the calculations with the N-processes included yielded a peak at much lower temperatures near 280 K. However, the calculations show that the inclusion of the N-processes does not yield the correct trend of the NW thermal conductivity. This suggests that normal phonon-phonon processes do not play an important role in governing thermal transport in nanostructures and may be neglected. As a result, thermal transport in NWs tends to the ballistic regime in which phonons move in almost straight lines before being scattered by the boundary. The effect of surface roughness was also apparent from the model results. The calculated thermal conductivities decreased with increasing surface roughness as expected, since increased surface roughness serves to increase phonon diffuse scattering at the surface. In addition, the thermal conductivity peaks were observed to shift to lower temperatures as the surface roughness was reduced. The measured thermal conductivity for the 22 nm diameter NW, did not exhibit a peak within the experimental temperature range. The model results showed that the thermal conductivity of the 22 nm diameter NW peaks in the temperature range between 540 and 650 K and the peak occurs at higher temperatures for the 10 nm wire, which is in agreement with the experimentally reported behavior.

A notable result of the model calculations is that the thermal conductance of a free surface NW is larger than that of a clamped NW. Clamping of the surface leads to phonon hardening (i.e the shifting of the dispersion branches to higher frequencies) resulting in a lower contribution to the thermal conductivity. The exact opposite occurs in the case of the free surface NWs. The thermal conductivity of a 22 nm diameter free surface NW was observed to be slightly higher

than that of the clamped NW. On the other hand, the thermal conductivity of the free surface 10 nm diameter NW was observed to almost double that of the clamped surface NW. The effect was notably enhanced in 10 nm NWs due to the increase in the surface to volume ratio.

The naturally low thermal conductivity of NWs could find applications in thermoelectric devices. The efficiency of thermoelectric devices depends on the thermoelectric figure of merit $ZT = S^2T/\rho\kappa$, where S is the Seebeck coefficient, ρ is the electrical resistivity, and κ and T are the thermal conductivity and absolute temperature. Hence, due to their low thermal conductivity it is expected that NWs would make highly efficient thermoelectric devices. Moreover, the strong dependence of the thermal conductivity in NWs on cross-section and its sensitivity to the surface roughness suggests that their thermal and electrical properties may be tuned through clever engineering of the wire surface. Measurements on thermal conductivity of electroless etched Si NWs [52] showed that the thermal conductivity of these rough NWs was drastically reduced in comparison to that of Si NWs that were synthesized by the VLS method. The authors showed that it is possible to achieve $ZT \approx 0.6$ at room temperature in etched Si NWs of 50 nm diameter, which is three orders of magnitude larger than that of bulk Si. The authors argue that with optimized doping, diameter reduction, and roughness control, the ZT is likely to rise even higher.

Further, the model results show that it might be possible to achieve thermal current modulation through the manipulation of the surface boundary conditions. The large difference between the thermal conductivities of a small diameter free surface NW and that of a clamped surface may be exploited to cause variations in the NW thermal current. The thermal current is proportional to the material thermal conductivity, so that any changes in the thermal conductivity will result in a variation of the thermal current. The bulk of energy in device components is carried by electrical currents. But, in fact a large fraction of the carried energy is always lost through Joule heating effects. Achieving control of the thermal current thus could represent a huge leap in improving the efficiency of these devices, and will be essential in creating thermal technological devices. Manipulation of the surface boundary conditions of NWs could be a viable way to achieve this task. The thermal current may be modulated and controlled by successively clamping and unclamping the NW surface. In section 5.3 we proposed a practical system for the implementation of thermal current modulation in NWs using a Piezoelectric cladding material (see Figure 5.11). According to the results of our model it is expected that future experimental study of the effects of surface conditions on the thermal conductivity of small diameter NWs (10 nm or less) will be an important step in realizing thermal current modulation and developing efficient thermal technological devices.

As a continuation of this work, an important exercise would be to investigate thermal transport in NWs by energy carriers other than pure phonon modes. A promising candidate for such an investigation are surface phonon-polariton modes which have been shown by Chen *et al* [53] to enhance the thermal conductance in thin films. The increase of thermal conductivity due to these modes is largly attributed to their long propagation lengths and mean free paths. Therefore, the study of heat conduction due to these modes in NWs may provide valuable insight into other forms of thermal current modulation and energy transfer enhancement. The model here presented may be easily modified to include the contribution of these modes.

Appendix A

Appendix

A.1 Derivation of the relaxation time due to impurity scattering

In order to derive the scattering rate due to mass difference scattering from (3.3.1) we must start by writing an expression for the crystal Hamiltonian. The harmonic part of the Hamiltonian can be written in the following canonical form in terms of creation and annihilation operators [2]:

$$H_{harm} = \sum_{\mathbf{k}s} \hbar\omega(\mathbf{k}s)(a^{\dagger}_{\mathbf{k}s}a_{\mathbf{k}s} + 1/2) \tag{A.1.1}$$

the creation and annihilation operators $a^{\dagger}_{\mathbf{k}s}$ and $a_{\mathbf{k}s}$ satisfy the relations

$$\begin{aligned} \left[a_{\mathbf{k}s}, a^{\dagger}_{\mathbf{k}'s'}\right] &= \delta_{\mathbf{k},\mathbf{k}'}\delta_{s,s'}\hat{\mathbf{I}} \\ a^{\dagger}_{\mathbf{k}s}\Psi_{N_{\mathbf{k}s}} &= \sqrt{N_{\mathbf{k}s}+1}\Psi_{N_{\mathbf{k}s}+1} \\ a_{\mathbf{k}s}\Psi_{N_{\mathbf{k}s}} &= \sqrt{N_{\mathbf{k}s}}\Psi_{N_{\mathbf{k}s}-1} \\ a^{\dagger}_{\mathbf{k}s}a_{\mathbf{k}s}\Psi_{N_{\mathbf{k}s}} &= N_{\mathbf{k}s}\Psi_{N_{\mathbf{k}s}} \end{aligned} \tag{A.1.2}$$

where $\Psi_{N_{\mathbf{k}s}}$ are eigenstates of the Hamiltonian (A.1.1). Thus in this formalism the operator $a^{\dagger}_{\mathbf{k}s}a_{\mathbf{k}s}$ is just the phonon number operator.

One way to study impurity scattering is to consider that the impurities are substantial atoms of different mass than the atoms making up the solid. Hence the solid Hamiltonian can be written in the following way

$$H = H_0 + H_{md} \tag{A.1.3}$$

where

$$H_0 = \sum_n \frac{1}{2}\overline{M}\dot{u}_n^2 \tag{A.1.4}$$

is the unperturbed part. And

$$H_{md} = \sum_n \frac{1}{2}(M_n - \overline{M})\dot{u}_n^2 = \sum_n \frac{1}{2}\Delta M_n \dot{u}_n^2 \tag{A.1.5}$$

is the perturbation due to mass difference.

Here

$$\overline{M} = \sum_i f_i M_i = \frac{1}{N_0}\sum_n M_n \tag{A.1.6}$$

is the average mass in the solid, with f_i the fraction of the unit cells having mass M_i, and N_0 is the number of unit cells in the solid.

In the low temperature limit the phonon wavelength is long so that the crystal can be considered as an elastic continuum. The displacement vector for an elastic continuum can also be written in quantized form [2]:

$$\mathbf{u}(\mathbf{r}) = -i\sqrt{\frac{\hbar}{2\rho V}}\sum_{\mathbf{k}s}\frac{1}{\sqrt{\omega(\mathbf{k}s)}}\mathbf{e}_{\mathbf{k}s}(a_{\mathbf{k}s}^\dagger - a_{-\mathbf{k}s})e^{i(\mathbf{k}.\mathbf{r}-\omega t)} \tag{A.1.7}$$

in which $\mathbf{e}_{\mathbf{k}s}$ are polarization vectors that satisfy the orthogonality relation

$$\int \mathbf{e}_{\mathbf{k}s}^*(\mathbf{r}).\mathbf{e}_{\mathbf{k}s'}(\mathbf{r})d^3\mathbf{r} = \delta_{ss'} \tag{A.1.8}$$

With this H_{md} becomes

$$H_{md} = \frac{\hbar}{4\rho V}\sum_{\mathbf{k}s}\sum_{\mathbf{k}'s'}\sqrt{\omega(\mathbf{k}s)\omega(\mathbf{k}'s')}\mathbf{e}_{\mathbf{k}s}^*.\mathbf{e}_{\mathbf{k}'s'}(a_{\mathbf{k}s}^\dagger - a_{-\mathbf{k}s})(a_{\mathbf{k}'s'}^\dagger - a_{-\mathbf{k}'s'})M_{\mathbf{k}\mathbf{k}'} \tag{A.1.9}$$

$$= \sum_{\mathbf{k}s}\sum_{\mathbf{k}'s'} H_{md}(\mathbf{k}s, \mathbf{k}'s') \tag{A.1.10}$$

where,

$$M_{\mathbf{k}\mathbf{k}'} = \sum_n \Delta M_n e^{i(\mathbf{k}-\mathbf{k}').\mathbf{r}_n} \tag{A.1.11}$$

Using Fermi's golden rule we can find the transition probability between an initial state $\Psi_{N_{\mathbf{k}s}}^{N_{\mathbf{k}'s'}}$ and a final state $\Psi_{N_{\mathbf{k}s}-1}^{N_{\mathbf{k}'s'}+1}$:

$$P_{\mathbf{k}s}^{\mathbf{k}'s'} = \frac{2\pi}{\hbar}\left|\left(\Psi_{N_{\mathbf{k}s}-1}^{N_{\mathbf{k}'s'}+1}, H_{md}(\mathbf{k}s,\mathbf{k}'s')\Psi_{N_{\mathbf{k}s}}^{N_{\mathbf{k}'s'}}\right)\right|^2 \delta\big(\omega(\mathbf{k}s)-\omega(\mathbf{k}'s')\big) \tag{A.1.12}$$

using the relations (A.1.2), and (A.1.10) we find

$$P_{\mathbf{k}s}^{\mathbf{k}'s'} = \frac{\pi}{2(\rho V)^2} N_{\mathbf{k}s}(N_{\mathbf{k}'s'}+1)\omega(\mathbf{k}s)\omega(\mathbf{k}'s')(\mathbf{e}_{\mathbf{k}s}^{*}.\mathbf{e}_{\mathbf{k}'s'})^2|M_{\mathbf{k}\mathbf{k}'}|^2\delta\big(\omega(\mathbf{k}s)-\omega(\mathbf{k}'s')\big) \tag{A.1.13}$$

If we assume that the isotopes or impurities are randomly distributed then we have

$$\begin{aligned}|M_{\mathbf{k}\mathbf{k}'}|^2 &= \sum_n (\Delta M_n)^2 + \sum_{n\neq n'} \Delta M_n \Delta M_{n'} e^{i(\mathbf{k}-\mathbf{k}').(\mathbf{r}_n-\mathbf{r}_{n'})} \\ &= \sum_n (\Delta M_n)^2 = N_0 \sum_i f_i (\Delta M_n)^2 \end{aligned} \tag{A.1.14}$$

The second term in the first line of (A.1.14) vanishes for a random distribution. Then

$$P_{\mathbf{k}s}^{\mathbf{k}'s'} = \frac{\pi\Gamma_{md}}{2N_0} N_{\mathbf{k}s}(N_{\mathbf{k}'s'}+1)\omega(\mathbf{k}s)\omega(\mathbf{k}'s')(\mathbf{e}_{\mathbf{k}s}^{*}.\mathbf{e}_{\mathbf{k}'s'})^2\delta\big(\omega(\mathbf{k}s)-\omega(\mathbf{k}'s')\big) \tag{A.1.15}$$

In which

$$\Gamma_{md} = \sum_i f_i \left(\frac{\Delta M_i}{\overline{M}}\right)^2 \tag{A.1.16}$$

The transition probability in the backward direction $P_{\mathbf{k}'s'}^{\mathbf{k}s}$ can be obtained from (A.1.15) by the exchange $\mathbf{k}s \longleftrightarrow \mathbf{k}'s'$.

The scattering term due to mass difference scattering in this case is given by

$$\begin{aligned}\frac{N_{\mathbf{k}s}}{\partial t}\Big|_{md} &= \sum_{\mathbf{k}'s'}[P_{\mathbf{k}'s'}^{\mathbf{k}s} - P_{\mathbf{k}s}^{\mathbf{k}'s'}] \\ &= \frac{\pi\Gamma_{md}}{2N_0}\sum_{\mathbf{k}'s'}[N_{\mathbf{k}'s'}(N_{\mathbf{k}s}+1) - N_{\mathbf{k}s}(N_{\mathbf{k}'s'}+1)] \\ &\times \omega(\mathbf{k}s)\omega(\mathbf{k}'s')(\mathbf{e}_{\mathbf{k}s}^{*}.\mathbf{e}_{\mathbf{k}'s'})^2\delta\big(\omega(\mathbf{k}s)-\omega(\mathbf{k}'s')\big) \\ &= \frac{\pi\Gamma_{md}}{2N_0}\sum_{\mathbf{k}'s'}[(N_{\mathbf{k}'s'}-\overline{N}_{\mathbf{k}'s'}) - (N_{\mathbf{k}s}-\overline{N}_{\mathbf{k}s})] \\ &\times \omega(\mathbf{k}s)\omega(\mathbf{k}'s')(\mathbf{e}_{\mathbf{k}s}^{*}.\mathbf{e}_{\mathbf{k}'s'})^2\delta\big(\omega(\mathbf{k}s)-\omega(\mathbf{k}'s')\big)\end{aligned} \tag{A.1.17}$$

using (2.3.3) and the fact that $\overline{N}_{\mathbf{k}s} = \overline{N}_{\mathbf{k}'s'}$ which is true for an elastic process with $\omega(\mathbf{k}s) = \omega(\mathbf{k}'\mathbf{s}')$, the scattering term (A.1.17) can be written as

$$\frac{N_{\mathbf{k}s}}{\partial t}\Big|_{md} = \frac{\pi\Gamma_{md}}{2N_0}\sum_{\mathbf{k}'s'}(\psi_{\mathbf{k}'s'} - \psi_{\mathbf{k}s})\overline{N}_{\mathbf{k}s}(\overline{N}_{\mathbf{k}'s'}+1)\omega(\mathbf{k}s)\omega(\mathbf{k}'s')(\mathbf{e}^*_{\mathbf{k}s}.\mathbf{e}_{\mathbf{k}'s'})^2 \times \delta\big(\omega(\mathbf{k}s) - \omega(\mathbf{k}'s')\big) \tag{A.1.18}$$

The expression for the single mode relaxation time can be obtained by setting $\psi_{\mathbf{k}'s'}(\mathbf{k}'s' \neq \mathbf{k}s) = 0$ in (A.1.18):

$$\begin{aligned}\frac{N_{\mathbf{k}s}}{\partial t}\Big|_{md} &= -\frac{\pi\Gamma_{md}}{2N_0}\sum_{\mathbf{k}'s'}\psi_{\mathbf{k}s}\overline{N}_{\mathbf{k}s}(\overline{N}_{\mathbf{k}'s'}+1)\omega(\mathbf{k}s)\omega(\mathbf{k}'s')(\mathbf{e}^*_{\mathbf{k}s}.\mathbf{e}_{\mathbf{k}'s'})^2 \\ &\quad\times\delta\big(\omega(\mathbf{k}s) - \omega(\mathbf{k}'s')\big) \\ &= -\frac{\psi_{\mathbf{k}s}\overline{N}_{\mathbf{k}s}(\overline{N}_{\mathbf{k}'s'}+1)}{\tau_{md}(\mathbf{k}s)}\end{aligned} \tag{A.1.19}$$

Whence the relaxation time due mass difference scattering is

$$\tau^{-1}_{md}(\mathbf{k}s) = \frac{\pi\Gamma_{md}}{2N_0}\sum_{\mathbf{k}'s'}\omega(\mathbf{k}s)\omega(\mathbf{k}'s')(\mathbf{e}^*_{\mathbf{k}s}.\mathbf{e}_{\mathbf{k}'s'})^2\delta\big(\omega(\mathbf{k}s) - \omega(\mathbf{k}'s')\big) \tag{A.1.20}$$

Changing the summation into integration the relaxation time (A.1.20) reads

$$\begin{aligned}\tau^{-1}_{md} &= \frac{\pi\Gamma_{md}V_u}{4\pi^2}\sum_{s'}\int dk'k'^2\omega(\mathbf{k}s)\omega(\mathbf{k}'s')(\mathbf{e}^*_{\mathbf{k}s}.\mathbf{e}_{\mathbf{k}'s'})^2\delta\big(\omega(\mathbf{k}s) - \omega(\mathbf{k}'s')\big) \\ &= \frac{\Gamma_{md}V_u}{4\pi}\sum_{s'}\frac{1}{v^3_{s'}}\int d\omega'\omega'^2\omega(\mathbf{k}s)\omega(\mathbf{k}'s')(\mathbf{e}^*_{\mathbf{k}s}.\mathbf{e}_{\mathbf{k}'s'})^2\delta\big(\omega(\mathbf{k}s) - \omega(\mathbf{k}'s')\big) \\ &= \frac{\Gamma_{md}V_u}{4\pi}\sum_{s'}\frac{1}{v^3_{s'}}\omega(\mathbf{k}s)^4(\mathbf{e}^*_{\mathbf{k}s}.\mathbf{e}_{\mathbf{k}s})^2\end{aligned} \tag{A.1.21}$$

where V_u is the volume per unit cell, v is the phonon group velocity.

The factor $(\mathbf{e}^*_{\mathbf{k}s}.\mathbf{e}_{\mathbf{k}s})^2$ can be approximated to be 1/3 for an isotropic solid so that the relaxation time due to mass difference scattering can be written as

$$\tau^{-1}_{md} = \frac{\Gamma_{md}V_u}{4\pi\overline{v}^3}\omega^4 \tag{A.1.22}$$

where $3/\overline{v}^3 = \sum_s v_s^{-3}$.

Klemens [64] suggested the following expression for Γ_{md} for the general case of an impurity:

$$\Gamma_{md} = \sum_i f_i[(\Delta M_i/M)^2 + 2(\Delta g_i/g - 6.4\gamma\Delta\delta_i/\delta)^2] \tag{A.1.23}$$

where δ_i is the radius of the impurity atom in the host lattice, δ is the radius of an atom in the virtual crystal, g_i is an average stiffness constant of nearest-neighbor bonds from the impurity to the host lattice, g is the average stiffness constant for the host atoms, $\Delta g_i = g_i - g$, $\Delta\delta_i = \delta_i - \delta$, and γ is an average anharmonicity of the bonds.

Bibliography

[1] S. Volz, *Thermal nanosystems and nanomaterials*, vol. 118. Springer Science & Business Media, 2009.

[2] G. P. Srivastava, *The physics of phonons*. CRC press, 1990.

[3] D. Morelli, J. Heremans, and G. Slack, "Estimation of the isotope effect on the lattice thermal conductivity of group iv and group iii-v semiconductors," *Physical Review B*, vol. 66, no. 19, p. 195304, 2002.

[4] D. Li, Y. Wu, P. Kim, L. Shi, P. Yang, and A. Majumdar, "Thermal conductivity of individual silicon nanowires," *Applied Physics Letters*, vol. 83, no. 14, pp. 2934–2936, 2003.

[5] G. Chen, "Particularities of heat conduction in nanostructures," *Journal of Nanoparticle Research*, vol. 2, no. 2, pp. 199–204, 2000.

[6] B. Li and J. Wang, "Anomalous heat conduction and anomalous diffusion in one-dimensional systems," *Physical review letters*, vol. 91, no. 4, p. 044301, 2003.

[7] A. Dhar, "Heat transport in low-dimensional systems," *Advances in Physics*, vol. 57, no. 5, pp. 457–537, 2008.

[8] C.-L. Tien and G. Chen, "Challenges in microscale conductive and radiative heat transfer," *Journal of Heat Transfer*, vol. 116, no. 4, pp. 799–807, 1994.

[9] P. K. Schelling, S. R. Phillpot, and P. Keblinski, "Comparison of atomic-level simulation methods for computing thermal conductivity," *Physical Review B*, vol. 65, no. 14, p. 144306, 2002.

[10] B. C. Daly, H. J. Maris, K. Imamura, and S. Tamura, "Molecular dynamics calculation of the thermal conductivity of superlattices," *Physical review B*, vol. 66, no. 2, p. 024301, 2002.

[11] Y. Chen, D. Li, J. R. Lukes, Z. Ni, and M. Chen, "Minimum superlattice thermal conductivity from molecular dynamics," *Physical Review B*, vol. 72, no. 17, p. 174302, 2005.

[12] K. Termentzidis, S. Merabia, P. Chantrenne, and P. Keblinski, "Cross-plane thermal conductivity of superlattices with rough interfaces using equilibrium and non-equilibrium molecular dynamics," *International Journal of Heat and Mass Transfer*, vol. 54, no. 9-10, pp. 2014–2020, 2011.

[13] E. Landry and A. McGaughey, "Effect of interfacial species mixing on phonon transport in semiconductor superlattices," *Physical Review B*, vol. 79, no. 7, p. 075316, 2009.

[14] J. Turney, A. McGaughey, and C. Amon, "Assessing the applicability of quantum corrections to classical thermal conductivity predictions," *Physical Review B*, vol. 79, no. 22, p. 224305, 2009.

[15] M. Mohr, J. Maultzsch, E. Dobardžić, S. Reich, I. Milošević, M. Damnjanović, A. Bosak, M. Krisch, and C. Thomsen, "Phonon dispersion of graphite by inelastic x-ray scattering," *Physical Review B*, vol. 76, no. 3, p. 035439, 2007.

[16] P. Klemens, "Thermal conductivity and lattice vibrational modes," in *Solid state physics*, vol. 7, pp. 1–98, Elsevier, 1958.

[17] P. Carruthers, "Theory of thermal conductivity of solids at low temperatures," *Reviews of Modern Physics*, vol. 33, no. 1, p. 92, 1961.

[18] C. Herring, "Role of low-energy phonons in thermal conduction," *Physical Review*, vol. 95, no. 4, p. 954, 1954.

[19] J. M. Ziman, *Electrons and phonons: the theory of transport phenomena in solids*. Oxford university press, 1960.

[20] J. Callaway, "Model for lattice thermal conductivity at low temperatures," *Physical Review*, vol. 113, no. 4, p. 1046, 1959.

[21] M. Holland, "Analysis of lattice thermal conductivity," *Physical Review*, vol. 132, no. 6, p. 2461, 1963.

[22] W. Li, N. Mingo, L. Lindsay, D. A. Broido, D. A. Stewart, and N. A. Katcho, "Thermal conductivity of diamond nanowires from first principles," *Physical Review B*, vol. 85, no. 19, p. 195436, 2012.

[23] L. Lindsay, D. Broido, and N. Mingo, "Lattice thermal conductivity of single-walled carbon nanotubes: Beyond the relaxation time approximation and phonon-phonon scattering selection rules," *Physical Review B*, vol. 80, no. 12, p. 125407, 2009.

[24] L. Lindsay, D. Broido, and N. Mingo, "Flexural phonons and thermal transport in graphene," *Physical Review B*, vol. 82, no. 11, p. 115427, 2010.

[25] H. Casimir, "Note on the conduction of heat in crystals," *Physica*, vol. 5, no. 6, pp. 495–500, 1938.

[26] K. Fuchs, "The conductivity of thin metallic films according to the electron theory of metals," in *Mathematical Proceedings of the Cambridge Philosophical Society*, vol. 34, pp. 100–108, Cambridge University Press, 1938.

[27] R. Chambers, "The conductivity of thin wires in a magnetic field," *Proc. R. Soc. Lond. A*, vol. 202, no. 1070, pp. 378–394, 1950.

[28] R. Dingle, "The electrical conductivity of thin wires," *Proc. R. Soc. Lond. A*, vol. 201, no. 1067, pp. 545–560, 1950.

[29] Z. Wang and N. Mingo, "Absence of casimir regime in two-dimensional nanoribbon phonon conduction," *Applied Physics Letters*, vol. 99, no. 10, p. 101903, 2011.

[30] A. A. Balandin, "Thermal properties of graphene and nanostructured carbon materials," *Nature materials*, vol. 10, no. 8, p. 569, 2011.

[31] M. M. Sadeghi, M. T. Pettes, and L. Shi, "Thermal transport in graphene," *Solid State Communications*, vol. 152, no. 15, pp. 1321–1330, 2012.

[32] A. Mavrokefalos, M. T. Pettes, F. Zhou, and L. Shi, "Four-probe measurements of the in-plane thermoelectric properties of nanofilms," *Review of scientific instruments*, vol. 78, no. 3, p. 034901, 2007.

[33] J.-K. Yu, S. Mitrovic, D. Tham, J. Varghese, and J. R. Heath, "Reduction of thermal conductivity in phononic nanomesh structures," *Nature nanotechnology*, vol. 5, no. 10, p. 718, 2010.

[34] J. Tang, H.-T. Wang, D. H. Lee, M. Fardy, Z. Huo, T. P. Russell, and P. Yang, "Holey silicon as an efficient thermoelectric material," *Nano letters*, vol. 10, no. 10, pp. 4279–4283, 2010.

[35] L. Shi, D. Li, C. Yu, W. Jang, D. Kim, Z. Yao, P. Kim, and A. Majumdar, "Measuring thermal and thermoelectric properties of one-dimensional nanostructures using a microfabricated device," *Journal of heat transfer*, vol. 125, no. 5, pp. 881–888, 2003.

[36] A. I. Persson, Y. K. Koh, D. G. Cahill, L. Samuelson, and H. Linke, "Thermal conductance of inas nanowire composites," *Nano letters*, vol. 9, no. 12, pp. 4484–4488, 2009.

[37] F. Zhou, A. L. Moore, J. Bolinsson, A. Persson, L. Fröberg, M. T. Pettes, H. Kong, L. Rabenberg, P. Caroff, D. A. Stewart, *et al.*, "Thermal conductivity of indium arsenide nanowires with wurtzite and zinc blende phases," *Physical Review B*, vol. 83, no. 20, p. 205416, 2011.

[38] A. Mavrokefalos, A. L. Moore, M. T. Pettes, L. Shi, W. Wang, and X. Li, "Thermoelectric and structural characterizations of individual electrodeposited bismuth telluride nanowires," *Journal of Applied Physics*, vol. 105, no. 10, p. 104318, 2009.

[39] L. Shi, Q. Hao, C. Yu, N. Mingo, X. Kong, and Z. L. Wang, "Thermal conductivities of individual tin dioxide nanobelts," in *ASME 2004 Heat Transfer/Fluids Engineering Summer Conference*, pp. 457–461, American Society of Mechanical Engineers, 2004.

[40] A. L. Moore, M. T. Pettes, F. Zhou, and L. Shi, "Thermal conductivity suppression in bismuth nanowires," *Journal of Applied Physics*, vol. 106, no. 3, p. 034310, 2009.

[41] F. Zhou, A. L. Moore, M. T. Pettes, Y. Lee, J. H. Seol, Q. L. Ye, L. Rabenberg, and L. Shi, "Effect of growth base pressure on the thermoelectric properties of indium antimonide nanowires," *Journal of Physics D: Applied Physics*, vol. 43, no. 2, p. 025406, 2009.

[42] H. Kim, I. Kim, H.-j. Choi, and W. Kim, "Thermal conductivities of si 1-x ge x nanowires with different germanium concentrations and diameters," *Applied Physics Letters*, vol. 96, no. 23, p. 233106, 2010.

[43] Z. Wang and N. Mingo, "Diameter dependence of sige nanowire thermal conductivity," *Applied Physics Letters*, vol. 97, no. 10, p. 101903, 2010.

[44] L. Shi, "Thermal and thermoelectric transport in nanostructures and low-dimensional systems," *Nanoscale and Microscale Thermophysical Engineering*, vol. 16, no. 2, pp. 79–116, 2012.

[45] L. D. Landau and E. Lifshitz, "Theory of elasticity, vol. 7," *Course of Theoretical Physics*, vol. 3, p. 109, 1986.

[46] Z. Popovic, J. Spitzer, T. Ruf, M. Cardona, R. Nötzel, and K. Ploog, "Folded acoustic phonons in gaas/alas corrugated superlattices grown along the [311] direction," *Physical Review B*, vol. 48, no. 3, p. 1659, 1993.

[47] R. Bhadra, M. Grimsditch, I. K. Schuller, and F. Nizzoli, "Brillouin scattering from unsupported al films," *Physical Review B*, vol. 39, no. 17, p. 12456, 1989.

[48] M. Grimsditch, R. Bhadra, and I. K. Schuller, "Lamb waves in unsupported thin films: A brillouin-scattering study," *Physical review letters*, vol. 58, no. 12, p. 1216, 1987.

[49] W. P. Mason, *Physical acoustics: principles and methods*. Academic press, 2013.

[50] J. Zou and A. Balandin, "Phonon heat conduction in a semiconductor nanowire," *Journal of Applied Physics*, vol. 89, no. 5, pp. 2932–2938, 2001.

[51] A. McNamara, B. Lee, and Z. Zhang, "Quantum size effect on the lattice specific heat of nanostructures," *Nanoscale and Microscale Thermophysical Engineering*, vol. 14, no. 1, pp. 1–20, 2010.

[52] A. I. Hochbaum, R. Chen, R. D. Delgado, W. Liang, E. C. Garnett, M. Najarian, A. Majumdar, and P. Yang, "Enhanced thermoelectric performance of rough silicon nanowires," *Nature*, vol. 451, no. 7175, p. 163, 2008.

[53] D.-Z. A. Chen, A. Narayanaswamy, and G. Chen, "Surface phonon-polariton mediated thermal conductivity enhancement of amorphous thin films," *Physical Review B*, vol. 72, no. 15, p. 155435, 2005.

[54] M. Kazan, G. Guisbiers, S. Pereira, M. Correia, P. Masri, A. Bruyant, S. Volz, and P. Royer, "Thermal conductivity of silicon bulk and nanowires: Effects of isotopic composition, phonon confinement, and surface roughness," *Journal of Applied Physics*, vol. 107, no. 8, p. 083503, 2010.

[55] M. Born and K. Huang, *Dynamical theory of crystal lattices*. Clarendon press, 1954.

[56] M. Kazan and S. Volz, "Calculation of the lattice thermal conductivity in granular crystals," *Journal of Applied Physics*, vol. 115, no. 7, p. 073509, 2014.

[57] H. Carslaw and J. Jaeger, *Conduction of heat in solids: Oxford Science Publications*. Oxford, England, 1959.

[58] C. R. Tellier and A. J. Tosser, *Size effects in thin films*, vol. 2. Elsevier, 2016.

[59] G. Chen, *Nanoscale energy transport and conversion: a parallel treatment of electrons, molecules, phonons, and photons*. Oxford University Press, 2005.

[60] D. C. Gazis, "Three-dimensional investigation of the propagation of waves in hollow circular cylinders. i. analytical foundation," *The journal of the Acoustical Society of America*, vol. 31, no. 5, pp. 568–573, 1959.

[61] G. N. Watson, *A treatise on the theory of Bessel functions*. Cambridge university press, 1995.

[62] N. Mingo, "Calculation of si nanowire thermal conductivity using complete phonon dispersion relations," *Physical Review B*, vol. 68, no. 11, p. 113308, 2003.

[63] M. Kazan, "Application of houston's method to the calculation of the direction-dependent thermal conductivity in finite crystals at low temperatures," *Journal of Heat Transfer*, vol. 139, no. 10, p. 102004, 2017.

[64] P. Klemens, "The scattering of low-frequency lattice waves by static imperfections," *Proceedings of the Physical Society. Section A*, vol. 68, no. 12, p. 1113, 1955.

[65] D. G. Cahill, W. K. Ford, K. E. Goodson, G. D. Mahan, A. Majumdar, H. J. Maris, R. Merlin, and S. R. Phillpot, "Nanoscale thermal transport," *Journal of applied physics*, vol. 93, no. 2, pp. 793–818, 2003.

[66] A. Weathers and L. Shi, "Thermal transport measurement techniques for nanowires and nanotubes," *Annual Review of Heat Transfer*, vol. 16, no. 16, 2013.

[67] N. Li, J. Ren, L. Wang, G. Zhang, P. Hänggi, and B. Li, "Colloquium: Phononics: Manipulating heat flow with electronic analogs and beyond," *Reviews of Modern Physics*, vol. 84, no. 3, p. 1045, 2012.

[68] G. Chen, "Ballistic-diffusive heat-conduction equations," *Physical Review Letters*, vol. 86, no. 11, p. 2297, 2001.

[69] F. Alvarez, D. Jou, and A. Sellitto, "Phonon boundary effects and thermal conductivity of rough concentric nanowires," *Journal of Heat Transfer*, vol. 133, no. 2, p. 022402, 2011.

[70] A. A. Maradudin, E. W. Montroll, G. H. Weiss, and I. Ipatova, *Theory of lattice dynamics in the harmonic approximation*, vol. 3. Academic press New York, 1963.

[71] D. P. Edward and I. Palik, "Handbook of optical constants of solids," 1985.

[72] A. M. Marconnet, M. A. Panzer, and K. E. Goodson, "Thermal conduction phenomena in carbon nanotubes and related nanostructured materials," *Reviews of Modern Physics*, vol. 85, no. 3, p. 1295, 2013.

[73] J. Callaway and H. C. von Baeyer, "Effect of point imperfections on lattice thermal conductivity," *Physical Review*, vol. 120, no. 4, p. 1149, 1960.

[74] A. L. Moore, S. K. Saha, R. S. Prasher, and L. Shi, "Phonon backscattering and thermal conductivity suppression in sawtooth nanowires," *Applied Physics Letters*, vol. 93, no. 8, p. 083112, 2008.

[75] D. Broido, M. Malorny, G. Birner, N. Mingo, and D. Stewart, "Intrinsic lattice thermal conductivity of semiconductors from first principles," *Applied Physics Letters*, vol. 91, no. 23, p. 231922, 2007.